NASA TECHNICAL NOTE

NASA TN D-5335

NASA TN D-5335

A FINITE-STEP METHOD FOR CALCULATION OF THEORETICAL LOAD DISTRIBUTIONS FOR ARBITRARY LIFTING-SURFACE ARRANGEMENTS AT SUBSONIC SPEEDS

by James A. Blackwell, Jr.

Langley Research Center
Langley Station, Hampton, Va.

NATIONAL AERONAUTICS AND SPACE ADMINISTRATION • WASHINGTON, D. C. • JULY 1969

1. Report No. NASA TN D-5335	2. Government Accession No.	3. Recipient's Catalog No.
4. Title and Subtitle A FINITE-STEP METHOD FOR CALCULATION OF THEORETICAL LOAD DISTRIBUTIONS FOR ARBITRARY LIFTING-SURFACE ARRANGEMENTS AT SUBSONIC SPEEDS		5. Report Date July 1969 6. Performing Organization Code
7. Author(s) James A. Blackwell, Jr.		8. Performing Organization Report No. L-5724
9. Performing Organization Name and Address NASA Langley Research Center Langley Station Hampton, Va. 23365		10. Work Unit No. 126-13-01-29-23 11. Contract or Grant No.
12. Sponsoring Agency Name and Address National Aeronautics and Space Administration Washington, D.C. 20546		13. Type of Report and Period Covered Technical Note 14. Sponsoring Agency Code

15. Supplementary Notes

16. Abstract

A simple theoretical method has been developed to compute the load distribution in subsonic compressible flow of arbitrary wings and lifting-surface arrangements. A finite-step method was used in the analysis. The results of the theoretical method have been compared with experiment and show good agreement.

17. Key Words Suggested by Author(s) Lifting-surface theory Nonplanar wings Pylons, end plates, fences Span load distribution	18. Distribution Statement Unclassified – Unlimited		
19. Security Classif. (of this report) Unclassified	20. Security Classif. (of this page) Unclassified	21. No. of Pages 40	22. Price* $3.00

*For sale by the Clearinghouse for Federal Scientific and Technical Information
Springfield, Virginia 22151

A FINITE-STEP METHOD FOR CALCULATION OF THEORETICAL LOAD DISTRIBUTIONS FOR ARBITRARY LIFTING-SURFACE ARRANGEMENTS AT SUBSONIC SPEEDS

By James A. Blackwell, Jr.
Langley Research Center

SUMMARY

This report presents a simple theoretical finite-step method for calculating the subsonic aerodynamic load distributions for arbitrary lifting-surface arrangements. The method may be applied to a wide variety of aerodynamic problems involving nonplanar wings, wing and pylons or end plates, wing and empennage, and biplanes. The results of the theoretical method have been compared with experiment and show good agreement in all cases. Applications of the method have been made for a series of illustrative examples.

INTRODUCTION

Much research is presently being devoted to increasing the range factors of subsonic cruise airplanes. In order to achieve better range factors through increased aerodynamic efficiency of the airplane design, wings of thinner sections and of increased sweep are being used which generally result in additional structural considerations. To produce an efficient aerodynamic and structural airplane design, an accurate prediction of the aerodynamic forces and their distribution over the wing and other lifting surfaces is desirable.

The results of an accurate theoretical calculation of the lift distribution for a wing alone (e.g., ref. 1) are partially invalidated by the presence of a fuselage, pylons, or nacelles. The experimental results given in references 2 and 3 indicate the magnitude of the interference effect of a vertical surface such as a fence or end plate on the span load distribution of a wing. It is shown in these references that the interference effect is substantial and should be taken into account. In the airplane design, when the structural stresses are required, approximate methods have generally been used to determine the lift distributions for interference problems. References 4 and 5 give examples of such procedures. Generally, interference solutions are mathematically complex, are restricted to particular configurations, and involve much computational labor to obtain an answer of

satisfactory accuracy. (See, for instance, refs. 6 and 7 in which the calculated interference loads due to end plates and tip tanks, respectively, are shown.)

It is the purpose of the present report to describe a simple method of lift-distribution calculation that is mathematically less complex than existing methods and can be applied to arbitrary wings and lifting-surface arrangements (i.e., wing and end plates, biplanes, wing and pylons, etc.). The method that is used for this analysis follows closely the finite-step method used by Campbell (ref. 8) for calculating wing-alone spanwise lift distributions. This concept involves using 2N rectangular horseshoe vortices placed along the quarter-chord lines of the lifting surfaces and equating the velocity from the total vortex system at the three-quarter-chord line to the component of free-stream velocity normal to the lifting surface to form 2N equations in 2N unknowns.

The method is developed in detail and formulas facilitating solution for the span load distribution and various other aerodynamic parameters are presented. Applications of the method have been made to various lifting-surface combinations with particular emphasis placed on a horizontal-wing—vertical-surface configuration. Comparison of the results obtained by the present method with experimental data are made.

SYMBOLS

A aspect ratio, $\frac{b^2}{S}$

b wing span, feet (meters)

b_H horizontal-tail span, feet (meters)

C_{Di} total induced drag coefficient, $\frac{D_i}{\frac{1}{2}\rho V_\infty^2 S}$

C_L horizontal-surface lift coefficient, $\frac{L}{\frac{1}{2}\rho V_\infty^2 S}$

C_{L_α} horizontal-surface lift-curve slope per radian, $\frac{\partial C_L}{\partial \alpha}$

C_Y vertical-surface side-force coefficient, $\frac{F_Y}{\frac{1}{2}\rho V_\infty^2 S_{VS}}$

C_{Y_α} vertical-surface side-force-curve slope per radian, $\frac{\partial C_Y}{\partial \alpha}$

c local streamwise chord, feet (meters)

c_{av} average chord, $\frac{\text{Area of surface}}{\text{Span of surface}}$, feet (meters)

c_l horizontal-surface section lift coefficient, $\frac{2\Gamma}{V_\infty c}$

c_{l_α} horizontal-surface section lift-curve slope per radian, $\frac{\partial c_l}{\partial \alpha}$

c_y vertical-surface section side-force coefficient, $\frac{2\Gamma}{V_\infty c}$

D_i total induced drag, pounds (newtons)

e efficiency factor

F_u backwash influence function, foot^{-1} (meter^{-1})

F'_u defined by equation (6)

F_v sidewash influence function, foot^{-1} (meter^{-1})

F'_v defined by equation (8)

F_w downwash influence function, foot^{-1} (meter^{-1})

F'_w defined by equation (11)

F_Y vertical-surface side force, pounds (newtons)

i local deflection at control point in PQ-plane, radians unless otherwise indicated

L horizontal-surface lift, pounds (newtons)

l vertical-surface height, feet (meters)

M one-half of number of rectangular horseshoe vortices spread over horizontal lifting surface

M_∞ free-stream Mach number

N one-half of total number of rectangular horseshoe vortices spread over entire airplane configuration

P_n coordinate of a particular horseshoe vortex

P_ν coordinate of a particular control point

p,q,r coordinates of point on lifting surface in P,Q,R axis system, feet (meters)

$p' = \frac{p}{\sqrt{1 - M_\infty^2}}$

S area of horizontal lifting surface, $feet^2$ ($meters^2$)

S_{VS} area of vertical surface, $feet^2$ ($meters^2$)

s semiwidth of horseshoe vortex, feet (meters)

u backwash velocity, in p-direction, feet/second (meters/second)

V_∞ free-stream velocity, feet/second (meters/second)

$V_\perp$ velocity from vortex system normal to lifting surface at control point, feet/second (meters/second)

v sidewash velocity, in q-direction, feet/second (meters/second)

w downwash velocity, in r-direction, feet/second (meters/second)

X,P longitudinal reference axes

x,y,z coordinates of point on lifting surface with respect to given horseshoe vortex in X,Y,Z axis system (see eq. (3)), feet (meters)

$x' = \frac{x}{\sqrt{1 - M_\infty^2}}$

Y,Q lateral reference axes

Z,R	vertical reference axes
α	local angle of attack at control point in PR-plane, radians unless otherwise indicated
Γ	circulation strength, feet^2/second (meters^2/second)
$\Gamma' = \frac{\Gamma}{4\pi V_\infty}$	
ζ	vertical location of lifting-surface root quarter-chord line, measured from origin in r-direction, feet (meters)
η	spanwise location of vertical surface, measured from origin, feet (meters)
Λ	sweep angle of quarter-chord line, degrees
λ	taper ratio, $\frac{\text{Tip chord}}{\text{Root chord}}$
ξ	longitudinal location of lifting-surface root quarter-chord line, measured from origin in p-direction, feet (meters)
ρ	mass density of air, slugs/foot^3 (kilograms/meter^3)
ϕ	angle of lifting surface in QR-plane, degrees

Subscripts:

H	horizontal tail
n	number designating a particular horseshoe vortex
vs	vertical surface
W	wing
ν	number designating a particular control point

ANALYSIS

Basic Concepts

In order to calculate the subsonic span loading of an arbitrary arrangement of lifting surfaces, the lifting surfaces are represented by a system of rectangular horseshoe vortices (fig. 1). For the present analysis, one horseshoe vortex along the chord is used. That is, the midpoints of the vortices are placed only at points along the quarter-chord lines. An equal number of control points are located along the three-quarter-chord lines.

The velocity from the total vortex system is equated to the component of free-stream velocity normal to the lifting surface chord at each control point. Application of this tangent-flow boundary condition for a symmetrical loading provides a set of N simultaneous equations in the N unknown circulation strengths. Solution of this set of equations provides the loading distributions over the lifting surfaces.

Derivation of Method

Backwash.- By utilizing the fundamental laws of induced velocity given in reference 9 for calculating the induced velocities from a line vortex, the backwash velocity induced at a control point P_ν by a singular rectangular horseshoe vortex (fig. 1) on a lifting surface of dihedral angle ϕ may be derived and is given by the expression

$$u\left(p'_\nu, q_\nu, r_\nu\right) = \frac{\Gamma}{4\pi} F_u(x', y, z, s, \phi) \tag{1}$$

where

$$F_u(x', y, z, s, \phi) = \frac{z\cos\phi - y\sin\phi}{(x')^2 + (z\cos\phi - y\sin\phi)^2}\left\{\frac{(y + s\cos\phi)\cos\phi + (z + s\sin\phi)\sin\phi}{\left[(x')^2 + (y + s\cos\phi)^2 + (z + s\sin\phi)^2\right]^{1/2}}\right.$$

$$\left. - \frac{(y - s\cos\phi)\cos\phi + (z - s\sin\phi)\sin\phi}{\left[(x')^2 + (y - s\cos\phi)^2 + (z - s\sin\phi)^2\right]^{1/2}}\right\} \tag{2}$$

and

$$\left.\begin{aligned} x' &= p'_\nu - p'_n \\ y &= q_\nu - q_n \\ z &= r_\nu - r_n \end{aligned}\right\} \tag{3}$$

The Prandtl-Glauert correction factor is applied to the p- and x-coordinates to account for compressibility effects.

By distributing 2N horseshoe vortices having 2N control points over the lifting surfaces (fig. 1), the backwash velocity at any of the control points P_ν which results from the 2N horseshoe vortices is

$$u(p'_\nu, q_\nu, r_\nu) = \frac{1}{4\pi} \sum_{n=1}^{2N} \Gamma_n F_{u,\nu n} \tag{4}$$

For symmetrical geometry with respect to the PR-plane, the backwash velocity at any of the control points P_ν becomes

$$u(p'_\nu q_\nu r_\nu) = \frac{1}{4\pi} \sum_{n=1}^{N} \Gamma_n F'_{u,\nu n} \tag{5}$$

where the function $F'_{u,\nu n}$ is obtained by summing the influence of the vortices on the left side of the PR-plane and the influence of the vortices on the right side of the PR-plane, that is,

$$F'_{u,\nu n} = F_u\left[(p'_\nu - p'_n), (q_\nu - q_n), (r_\nu - r_n), s_n, \phi_n\right]\Big|_{\text{Right side}}$$

$$+ F_u\left[(p'_\nu - p'_n), (q_\nu + q_n), (r_\nu - r_n), s_n, -\phi_n\right]\Big|_{\text{Left side}} \tag{6}$$

Sidewash.- For symmetrical geometry with respect to the PR-plane, the sidewash velocity of any of the control points P_ν which results from the 2N horseshoe vortices is

$$v(p'_\nu, q_\nu, r_\nu) = \frac{1}{4\pi} \sum_{n=1}^{N} \Gamma_n F'_{v,\nu n} \tag{7}$$

with the function $F'_{v,\nu n}$ given by

$$F'_{v,\nu n} = F_v\left[(p_\nu - p_n), (q_\nu - q_n), (r_\nu - r_n), s_n, \phi_n\right]\Big|_{\text{Right side}}$$

$$+ F_v\left[(p_\nu - p_n), (q_\nu + q_n), (r_\nu - r_n), s_n, -\phi_n\right]\Big|_{\text{Left side}} \tag{8}$$

and

$$F_V(x',y,z,s,\phi) = \frac{x' \sin\phi}{(x')^2 + (z\cos\phi - y\sin\phi)^2}\left\{\frac{(y + s\cos\phi)\cos\phi + (z + s\sin\phi)\sin\phi}{\left[(x')^2 + (y + s\cos\phi)^2 + (z + s\sin\phi)^2\right]^{1/2}}\right.$$

$$\left. - \frac{(y - s\cos\phi)\cos\phi + (z - s\sin\phi)\sin\phi}{\left[(x')^2 + (y - s\cos\phi)^2 + (z - s\sin\phi)^2\right]^{1/2}}\right\}$$

$$+ \frac{z - s\sin\phi}{(y - s\cos\phi)^2 + (z - s\sin\phi)^2}\left\{1 - \frac{x'}{\left[(x')^2 + (y - s\cos\phi)^2 + (z - s\sin\phi)^2\right]^{1/2}}\right\}$$

$$- \frac{z + s\sin\phi}{(y + s\cos\phi)^2 + (z + s\sin\phi)^2}\left\{1 - \frac{x'}{\left[(x')^2 + (y + s\cos\phi)^2 + (z + s\sin\phi)^2\right]^{1/2}}\right\} \qquad (9)$$

Downwash.- For symmetrical geometry with respect to the PR-plane, the downwash velocity at any of the control points P_ν which results from the 2N horseshoe vortices is

$$w(p'_\nu, q_\nu, r_\nu) = \frac{1}{4\pi}\sum_{n=1}^{N} \Gamma_n F'_{w,\nu n} \qquad (10)$$

with the function $F'_{w,\nu n}$ given by

$$F'_{w,\nu n} = F_w\left[(p_\nu - p_n), (q_\nu - q_n), (r_\nu - r_n), s_n, \phi_n\right]\Big|_{\text{Right side}}$$

$$+ F_w\left[(p_\nu - p_n), (q_\nu + q_n), (r_\nu - r_n), s_n, -\phi_n\right]\Big|_{\text{Left side}} \qquad (11)$$

where

$$F_w(x',y,z,s,\phi) = \frac{-x' \cos\phi}{(x')^2 + (z\cos\phi - y\sin\phi)^2}\left\{\frac{(y + s\cos\phi)\cos\phi + (z + s\sin\phi)\sin\phi}{\left[(x')^2 + (y + s\cos\phi)^2 + (z + s\sin\phi)^2\right]^{1/2}}\right.$$

$$\left. - \frac{(y - s\cos\phi)\cos\phi + (z - s\sin\phi)\sin\phi}{\left[(x')^2 + (y - s\cos\phi)^2 + (z - s\sin\phi)^2\right]^{1/2}}\right\}$$

$$- \frac{y - s\cos\phi}{(y - s\cos\phi)^2 + (z - s\sin\phi)^2}\left\{1 - \frac{x'}{\left[(x')^2 + (y - s\cos\phi)^2 + (z - s\sin\phi)^2\right]^{1/2}}\right\}$$

$$+ \frac{y + s\cos\phi}{(y + s\cos\phi)^2 + (z + s\sin\phi)^2}\left\{1 - \frac{x'}{\left[(x')^2 + (y + s\cos\phi)^2 + (z + s\sin\phi)^2\right]^{1/2}}\right\} \quad (12)$$

To satisfy the tangent-flow boundary conditions, the velocity from the total vortex system normal to the lifting surface is equated to the component of free-stream velocity normal to the lifting surface at each control point such that there is no flow through the wing at the control points.

This boundary condition for a wing at dihedral ϕ at angle of attack (fig. 2(a)) may be expressed as

$$V_\perp = -v\sin\phi + w\cos\phi \quad (13)$$

For small angles of attack, the tangent-flow boundary condition may be expressed as

$$V_\perp\left(p'_\nu, q_\nu, r_\nu\right) = V_\infty \sin\alpha_\nu \cos\phi_\nu \approx V_\infty \alpha_\nu \cos\phi_\nu \quad (14)$$

Defining Γ'_n as $\Gamma_n/4\pi V_\infty$ and combining equations (7), (10), (13), and (14) yields

$$\alpha_\nu = \sum_{n=1}^{N} \Gamma'_n\left(F'_{w,\nu n} - F'_{v,\nu n}\tan\phi_\nu\right) \quad (15)$$

Similarly for a vertical-surface deflection i, the velocity from the vortex system normal to the vertical surface (fig. 2(b)) may be expressed as

$$V_\perp = -v\cos i + u\sin i \quad (16)$$

For small deflections and angles of attack, the tangent-flow boundary condition may be expressed as

$$V_{\perp}\left(p'_{\nu},q_{\nu},r_{\nu}\right) = V_{\infty} \cos \alpha_{\nu} \sin i_{\nu} \approx V_{\infty} i_{\nu} \tag{17}$$

Combining equations (4), (7), (16), and (17) yields

$$i_{\nu} = \sum_{n=1}^{N} \Gamma'_{n}\left(F'_{u,\nu n}\, i_{\nu} - F'_{v,\nu n}\right) \tag{18}$$

To determine the unknown circulation strengths Γ'_n on a combination of lifting surfaces, a set of N simultaneous equations in N unknown circulation strengths as given by equations (15) and (18) must be solved.

For a wing with dihedral ϕ and a pylon with incidence i, the system of equations to be solved is

$$\left.\begin{aligned} \sum_{\nu=1}^{M} \alpha_{\nu} &= \sum_{\nu=1}^{M} \sum_{n=1}^{N} \Gamma'_{n}\left(F'_{w,\nu n} - F'_{v,\nu n} \tan \phi_{\nu}\right) \\ \sum_{\nu=M+1}^{N} i_{\nu} &= \sum_{\nu=M+1}^{N} \sum_{n=1}^{N} \Gamma'_{n}\left(F'_{u,\nu n}\, i_{\nu} - F'_{v,\nu n}\right) \end{aligned}\right\} \tag{19}$$

Calculation of Loading Parameters

The formulas for calculating the airplane loading parameters vary with each airplane configuration. However, as an illustration, the formulas for calculation of the loading parameters for a horizontal wing and vertical surface (one on each wing half-span) are presented. Out of N control points on the wing half-span and vertical surface, the first M of these points are specified to be on the wing half-span and the remainder to be on the vertical surface.

Span loading coefficient.- By defining the wing span loading coefficient as $c_l c / C_L c_{av}$ and using the relation

$$\Gamma = \frac{c_l c V_{\infty}}{2} \tag{20}$$

the span loading coefficient on the wing may be obtained from the relation

$$\left(\frac{c_l c}{C_L c_{av}}\right)_n = \frac{\frac{b}{2}\Gamma'_n}{\sum_{n=1}^{M} \Gamma'_n 2s_n} \tag{21}$$

Similarly, the span loading coefficient on the vertical surfaces may be obtained from the relation

$$\left(\frac{c_y c}{C_Y c_{av}}\right)_n = \frac{l\Gamma'_n}{\sum_{n=M+1}^{N} \Gamma'_n 2s_n} \tag{22}$$

It should be noted that the circulation or span loading on the vertical surface at the vertical-surface—wing juncture may be determined from the boundary condition that specifies the circulation at the vertical-surface root to be equal to the difference between the circulation at stations inboard and outboard of the juncture.

Lift and side-force coefficients.- The lift of the wing may be expressed as

$$L = 2\int_0^{b/2} \rho V_\infty \Gamma(y)dy \tag{23}$$

Expressing the lift in coefficient form and simplifying gives

$$C_L = \frac{4}{V_\infty S}\int_0^{b/2} \Gamma(y)dy \tag{24}$$

Introducing Γ'_n and changing the integral to a summation results in

$$C_L = \frac{16\pi}{S}\sum_{n=1}^{M} \Gamma'_n 2s_n \tag{25}$$

Similarly, the side force of the vertical surface may be expressed as

$$F_Y = \int_0^{l} \rho V_\infty \Gamma(z)dz \tag{26}$$

or, in coefficient form, as

$$C_Y = \frac{8\pi}{S_{vs}}\sum_{n=M+1}^{N} \Gamma'_n 2s_n \tag{27}$$

DISCUSSION AND APPLICATION OF METHOD

Using the finite-step method, the spanwise load distribution as calculated for the wing alone is compared in figure 3 with the spanwise load distribution of a wing with a vertical surface attached to the wing lower surface at the 60-percent wing semispan. The calculations show that the addition of the vertical surface to the wing has a substantial effect on the wing spanwise loading.

The magnitude of the interference effects of lifting surfaces is dependent upon the geometry of the interfering lifting surfaces. In order to assess the interference effects of an arbitrary arrangement of lifting surfaces, equation (19) may be utilized.

To indicate the capability of the present method for predicting accurately the interference effects of arbitrary arrangements of lifting surfaces, comparisons are made with experimental data. In addition, several examples are presented to illustrate the range of applicability of the method.

Distribution of Vortices

The effect of the distribution of vortices spanwise over an arrangement of lifting surfaces on the aerodynamic loads as calculated by the present method is shown in figure 4 (symbols are used in fig. 4 to indicate distribution). As indicated in figure 4, the use of equal span vortices of semiwidth $\frac{s}{b/2} = 0.0250$ generally provided a satisfactory loading distribution. However, if there are regions of interest for which there are large gradients in the span load diagram, it has been found that a closer uniform spacing of vortices should be used. In all the following examples, a vortex semiwidth of $0.0250\frac{b}{2}$ is used unless otherwise stated. About 1 minute of computing time on the Control Data 6600 computer system (Langley program A1505) is generally required to obtain a solution when 50 vortices (2N) are used to describe the configuration.

Comparison of Theory With Experiment

A comparison of the calculated results for a 40° sweptback wing of $A_W = 4.5$ having a circular end plate with the experimental results as presented in reference 2 is shown in figure 5(a). A wing-alone comparison is also made in figure 5(b). Good agreement is shown with and without end plates.

The calculated results for a 45° sweptback wing of $A_W = 2.0$ with and without a fence are compared with the experimental results of reference 3 in figure 6 for constant total lift coefficients. The fence was located at $0.42\frac{b}{2}$ with a height of $0.12\frac{b}{2}$ above and below the wing. The agreement is shown to be good.

Examples

Vertical surfaces perpendicular to horizontal surfaces.- Examples of vertical surfaces perpendicular to horizontal surfaces include pylons, fences, end plates, and vertical tails perpendicular to wings. The location, number, sweep, and height of the vertical surfaces, in addition to Mach number and vertical-surface cant angle all affect the spanwise loading of a given wing. In the following illustrations, unless otherwise stated, the chords of the vertical surface are equal to the local wing chord; the wing is flat with $\Lambda_W = 30^o$, $\lambda_W = 0.33$, and $A_W = 6.67$; the vertical surface is at zero incidence with respect to the flight path and on the wing lower surface.

The effect of vertical-surface location on the wing spanwise loading is presented in figure 7(a). As the vertical surface is moved outboard, the magnitude of the drop in wing spanwise loading increases which in turn increases the loading on the vertical surface (fig. 7(b)). Since the chords for the vertical surfaces at various spanwise locations vary in figures 7 and 8, the parameter Γ_n' is presented instead of c_y to indicate the loading on the vertical surface. (It should be noted that $\Gamma_n' = \frac{c_y c}{8\pi}$.)

In figure 8, the effect of the number of vertical surfaces on the wing is shown. The drop and magnitude of the wing spanwise loading at the location of the vertical surfaces does not appear to be substantially altered by the number of vertical surfaces. Similarly the loading on the vertical surfaces remain essentially unchanged.

The sweep of the vertical surface primarily alters the vertical-surface loading (fig. 9). The loading for the sweptforward vertical surface rapidly drops off proceeding toward the tip of the vertical surface. This is a result of the sweep removing the tip of the vertical surface from the region of the wing influence.

The effect of vertical-surface height on the wing and vertical-surface loading is presented in figure 10. For vertical-surface heights of $\frac{l}{b/2} = 0.0$ to 0.2, the magnitude of the wing span load distribution appears to be generally proportional to the height of the vertical surface.

By using the Prandtl-Glauert transformation, the effect of Mach number on the wing and vertical-surface load distributions is determined and presented in figure 11.

Parallel lifting surfaces.- Biplanes, wing and horizontal tail, and wing and canard combination are examples of parallel lifting surfaces. As an example of the interference effect of parallel lifting surfaces, the effect of a wing on the lift of a horizontal tail is shown in figures 12 and 13. The lift coefficient of the horizontal tail is based on the horizontal-tail surface area. In figure 12, the lift distribution for a horizontal tail alone and a horizontal tail in the wake of a wing is presented. For the surface arrangement shown (tail with wing), the horizontal-tail lift coefficient is substantially reduced. The magnitude of the reduction in lift coefficient of the horizontal tail due to the interference

of the wing agrees with the reduction expected due to the change in tail angle of attack resulting from the downwash of the wing (see ref. 10 for empirical formulas for calculating the downwash angle at the wing-wake center line). In figure 13, the effect of horizontal-tail location behind a wing on the lift distribution of the horizontal tail is presented. Moving the tail vertically or further aft of the wing increases the horizontal-tail loading. For the horizontal-tail locations shown, there was negligible effect of the horizontal tail on the wing.

Optimum surfaces.- It is well known that if the span load distribution of a monoplane wing is elliptical, the induced drag of the monoplane wing will be a minimum, that is

$$C_{Di} = \frac{C_L{}^2}{\pi e A} \tag{28}$$

with $e = 1.00$. For lifting-surface arrangements other than the monoplane, it has been theoretically shown in references 5, 11, 12, and 13 that efficiency factors greater than 1 may be obtained and the optimum span load distribution is not necessarily elliptical. For example, the optimum wing span loading as given in reference 5 for a 30° sweptback wing with a sweptforward vertical surface having 75° of sweep, height $\frac{l}{b/2} = 0.2$, and located at $\frac{\eta}{b/2} = 0.6$ is presented in figure 14(a). The optimum vertical-surface loading for this configuration (fig. 14(b)) should be nearly elliptical (ref. 5). Shown also in figure 14 for comparison is the span and vertical-surface loading calculated by using the present method for the same wing at angle of attack with no twist and the same vertical-surface arrangement with zero deflection. Theoretically, $e = 1.025$ for this configuration with optimum loading. In figure 15, the approximate wing incidence and vertical-surface deflection as determined from the present method which would be required to achieve the optimum load distribution at a $C_L = 0.5$ are presented. It is interesting to note that for this configuration the differential twist outboard of the wing root and just inboard of the vertical surface is negligible. This is probably due to the vertical surface acting as an end plate, with the result that the area inboard of the vertical surface is more nearly two dimensional in character. For sweptforward vertical surfaces, the differential twist required to attain an elliptical load distribution on the vertical surface can be seen to be substantial (fig. 15(b)); however, for unswept vertical surfaces, probably very little differential twist would be required since the induced load is already very nearly elliptical (i.e., see fig. 9(b)).

CONCLUDING REMARKS

A simple theoretical finite-step method for calculating the subsonic aerodynamic load distributions for arbitrary lifting-surface arrangements has been developed. A wide

variety of aerodynamic problems involving nonplanar wings, wing and pylons or end plates, wing and empennage, and biplanes can be solved. The results of the theoretical method have been compared with experiment and show good agreement for the cases considered. Applications of the method have been made for a series of illustrative examples and good results are obtained.

Langley Research Center,
National Aeronautics and Space Administration,
Langley Station, Hampton, Va., May 22, 1969,
126-13-01-29-23.

REFERENCES

1. Multhopp, H.: Methods for Calculating the Lift Distribution of Wings (Subsonic Lifting-Surface Theory). R. & M. No. 2884, Brit. A.R.C., Jan. 1950.

2. Ingelmann-Sundberg, A. Martin M.: Experimental Determination of Pressure Distributions on a Plane Wing With 40° Sweepback at Low Speed. KTH-AERO TN 8, Div. Aeronaut., Roy. Inst. Technol. (Stockholm), 1949.

3. Weber, J.; and Lawford, J. A.: The Reflection Effect of Fences at Low Speeds. R. & M. No. 2977, Brit. A.R.C., 1956.

4. Schrenk, O.: A Simple Approximation Method for Obtaining the Spanwise Lift Distribution. NACA TM 948, 1940.

5. Weber, J.: Theoretical Load Distribution on a Wing With Vertical Plates. R. & M. No. 2960, Brit. A.R.C., 1956.

6. Robinson, A.: The Aerodynamic Loading of Wings With Endplates. R. & M. No. 2342, Brit. A.R.C., 1950.

7. Weber, J.: Theoretical Load Distribution on a Wing With a Cylindrical Body at One End. R. & M. No. 2889, Brit. A.R.C., 1957.

8. Campbell, George S.: A Finite-Step Method for the Calculation of Span Loadings of Unusual Plan Forms. NACA RM L50L13, 1951.

9. Glauert, H.: The Elements of Aerofoil and Airscrew Theory. Cambridge Univ. Press, 1937, pp. 125-160.

10. Dommasch, Daniel O.; Sherby, Sydney S.; and Connolly, Thomas F.: Airplane Aerodynamics. Second ed., Pitman Pub. Corp., 1957, p. 415.

11. Von Kármán, Th.; and Burgers, J. M.: General Aerodynamic Theory – Perfect Fluids. Vol. II of Aerodynamic Theory, div. E, W. F. Durand, ed., Julius Springer (Berlin), 1935 (reprinted by Durand Reprinting Comm., 1943).

12. Cone, Clarence D., Jr.: The Theory of Induced Lift and Minimum Induced Drag of Nonplanar Lifting Systems. NASA TR R-139, 1962.

13. Lundry, J. L.: A Numerical Solution for the Minimum Induced Drag, and the Corresponding Loading, of Nonplanar Wings. NASA CR-1218, 1968.

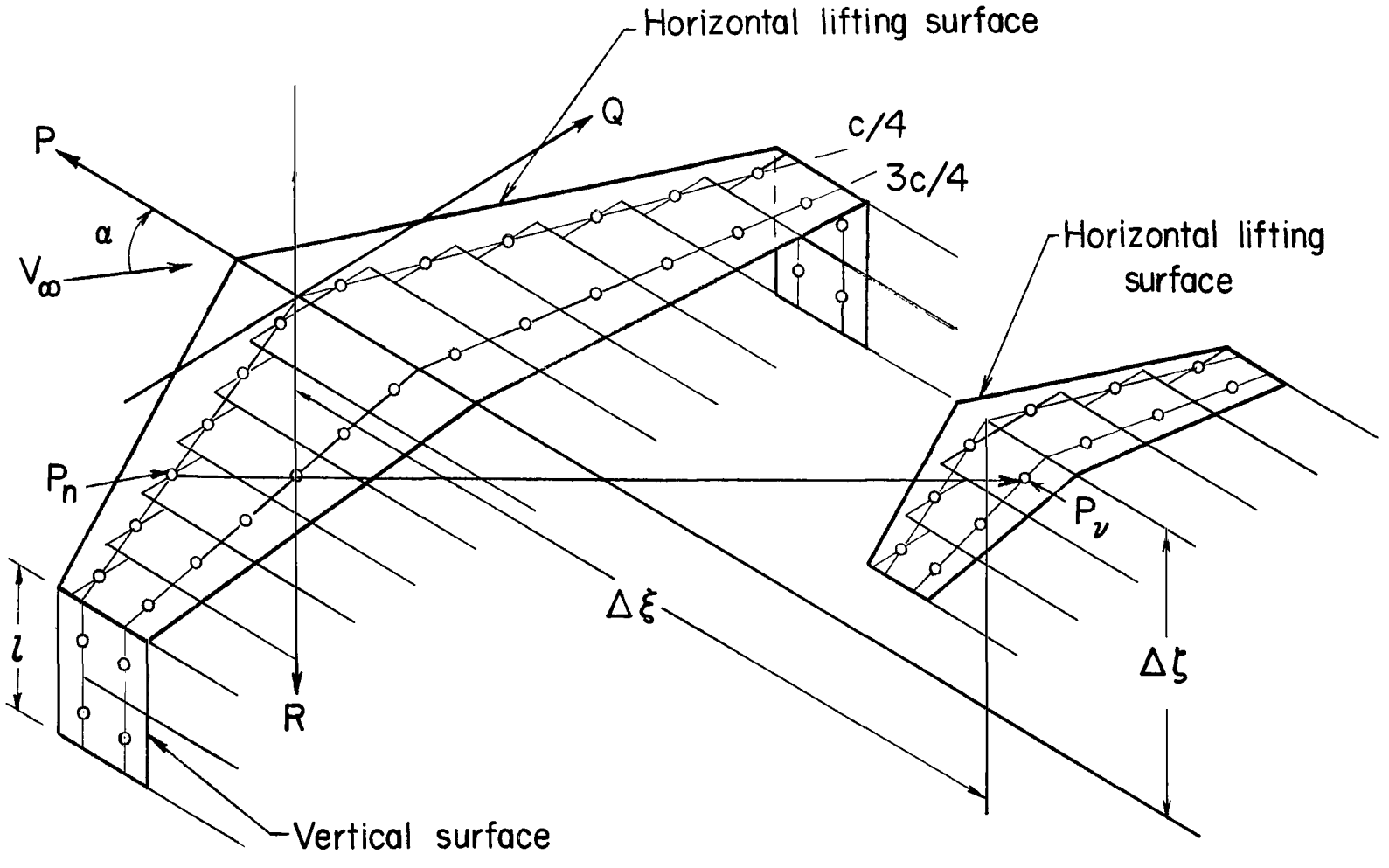

Figure 1.- Distribution of vortices over combination of lifting surfaces. N = 11.

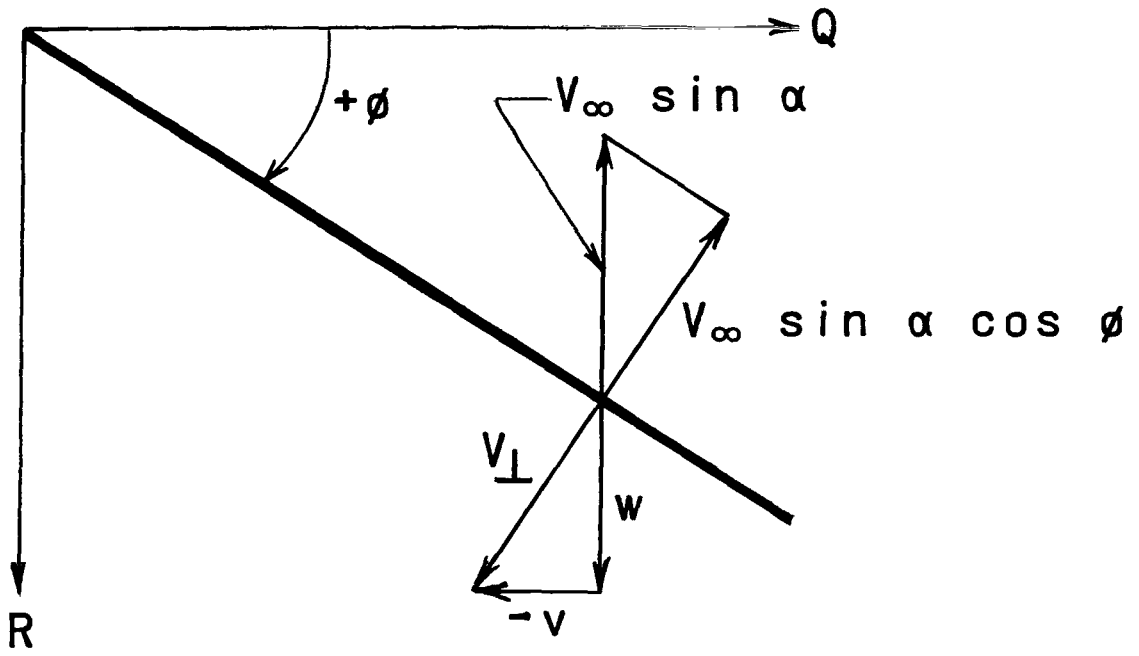

(a) Horizontal lifting surface.

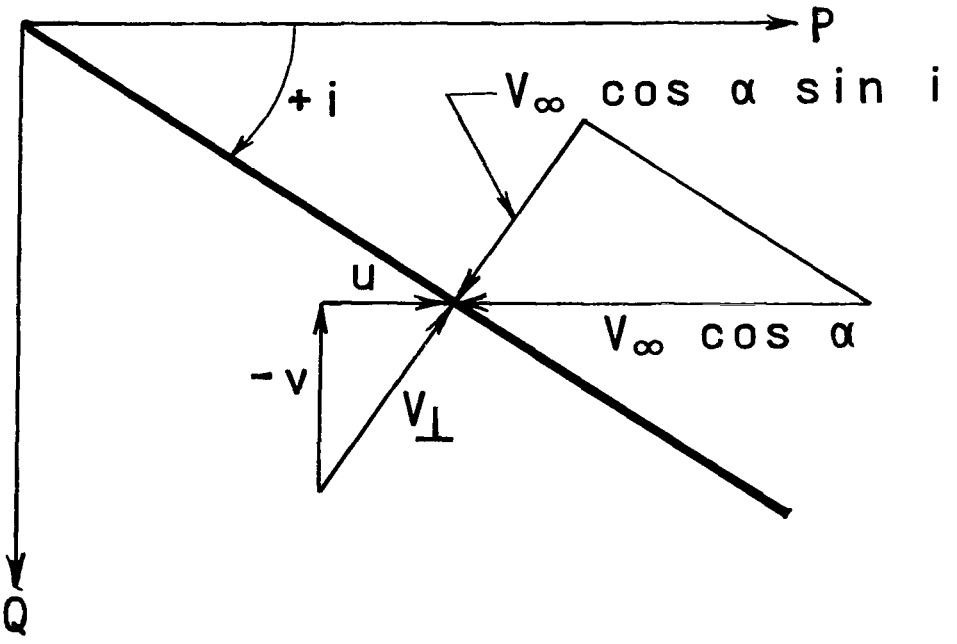

(b) Deflected vertical surface.

Figure 2.- Illustration of tangent-flow boundary condition.

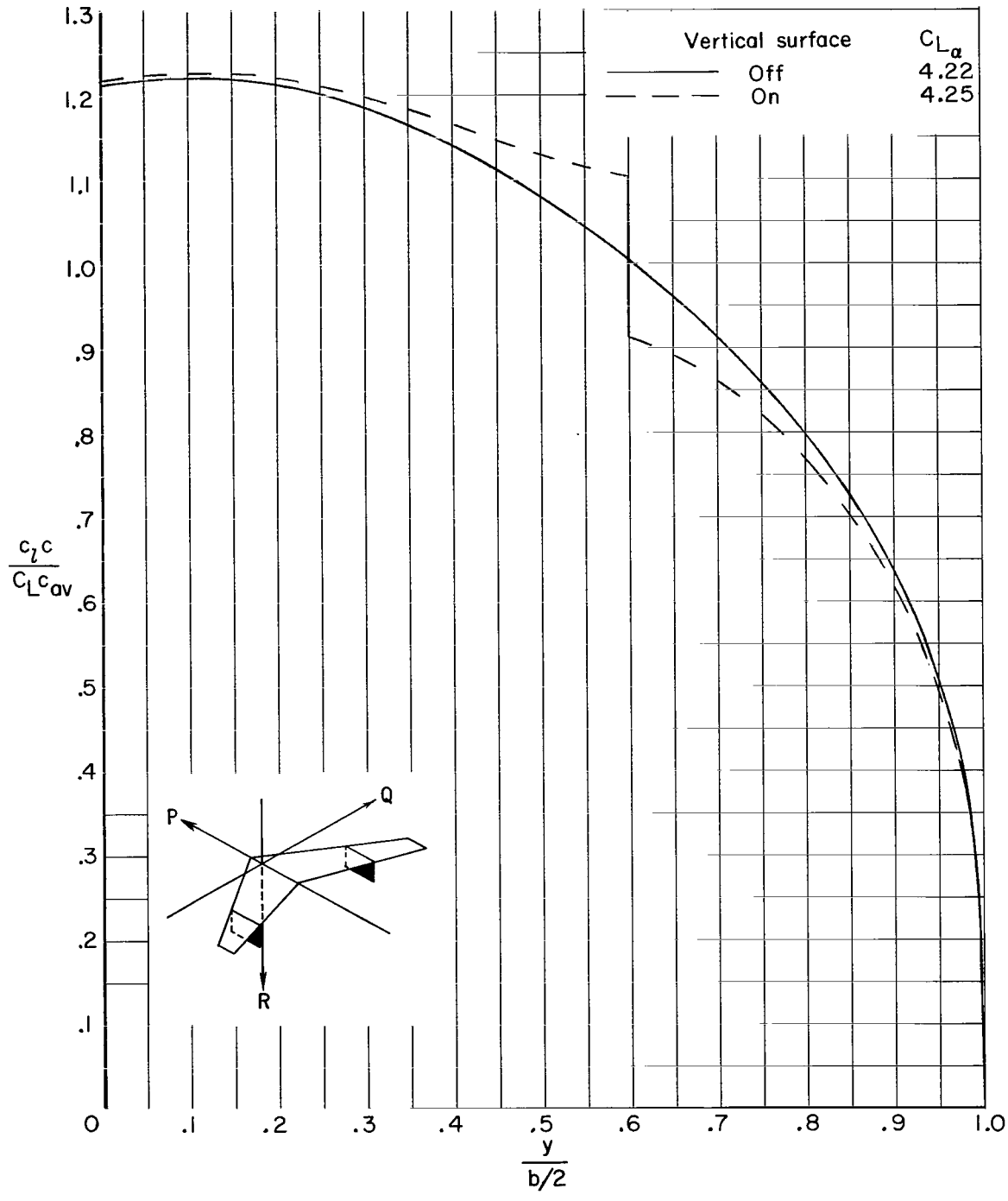

Figure 3.- Effect of vertical surface on spanwise loading of horizontal wing. $\Lambda_W = 30^0$; $A_W = 6.67$; $\lambda_W = 0.33$; $\Lambda_{VS} = 0^0$; $l = 0.2\frac{b}{2}$; $\eta = 0.6\frac{b}{2}$; $M_\infty = 0.0$; $s = 0.0250\frac{b}{2}$.

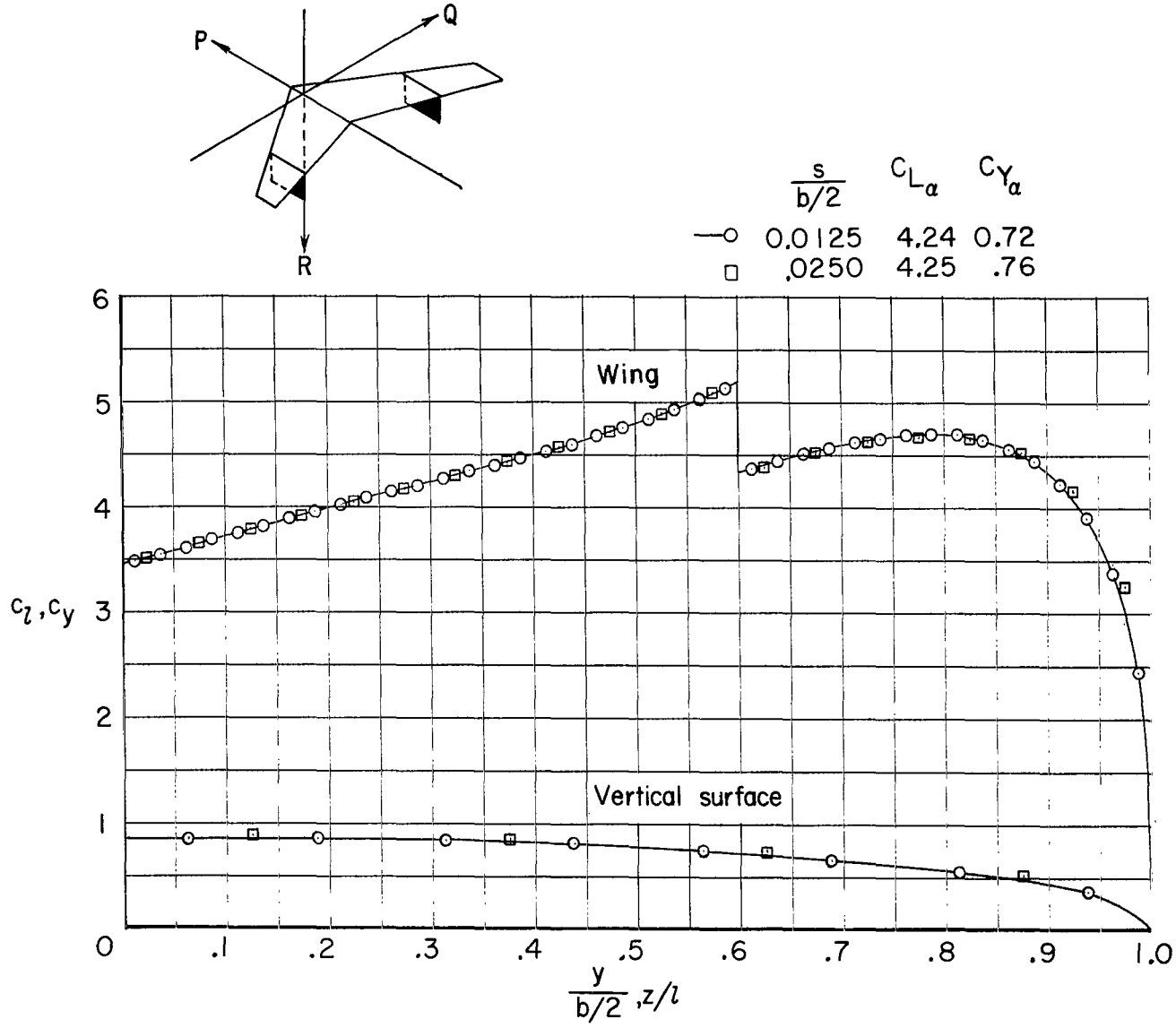

Figure 4.- Effect of distribution of vortices. $\Lambda_W = 30^0$; $A_W = 6.67$; $\lambda_W = 0.33$; $\Lambda_{VS} = 0^0$; $l = 0.2\frac{b}{2}$; $\eta = 0.6\frac{b}{2}$; $M_\infty = 0.0$; $\alpha = 1$ radian.

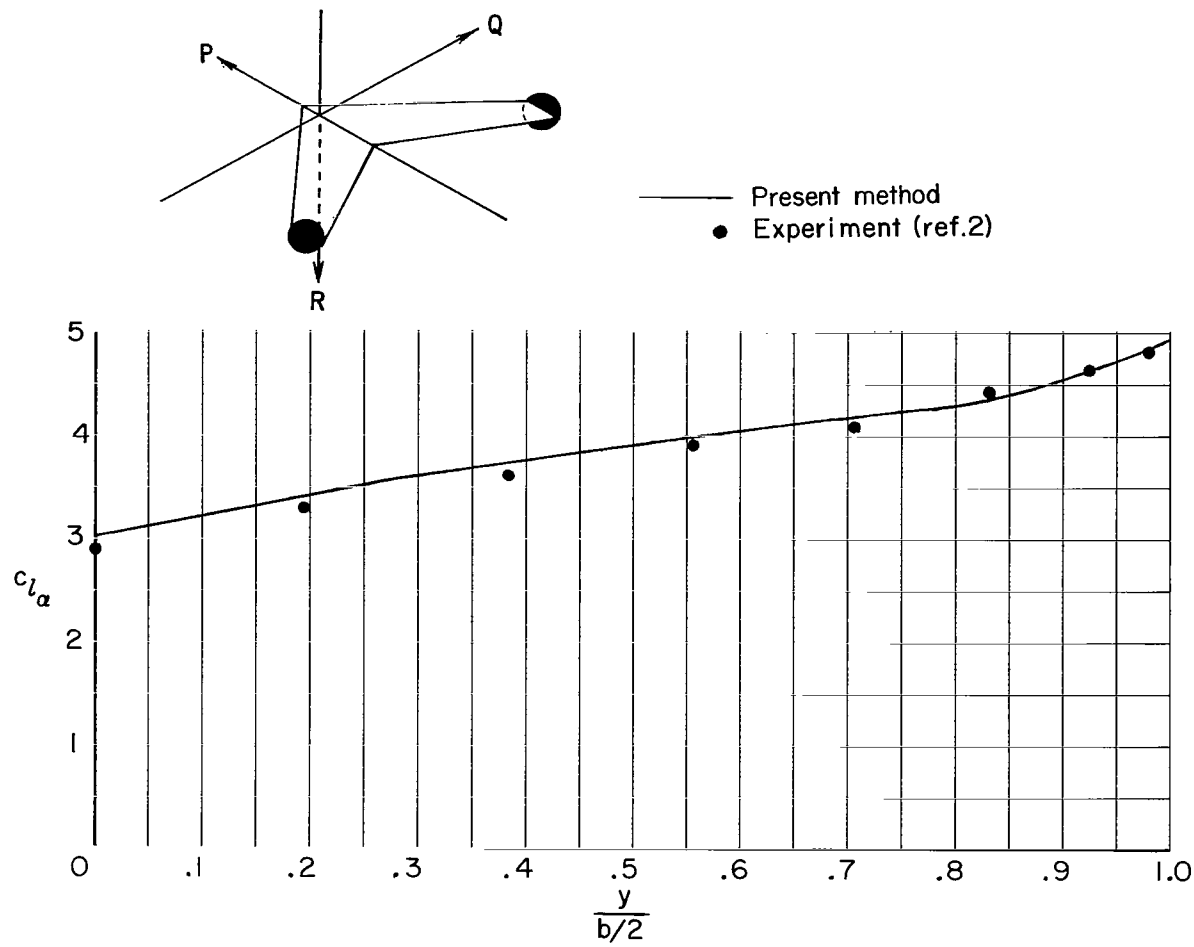

(a) Wing and end plate.

Figure 5.- Effect of end plate on section lift-curve slope as calculated by present method and as indicated by experimental data of reference 2. $\Lambda_W = 40^0$; $A_W = 4.5$; $\lambda_W = 0.5$; end plate circular with diameter equal to tip chord; $M_\infty \approx 0.1$; $s = 0.0250\frac{b}{2}$.

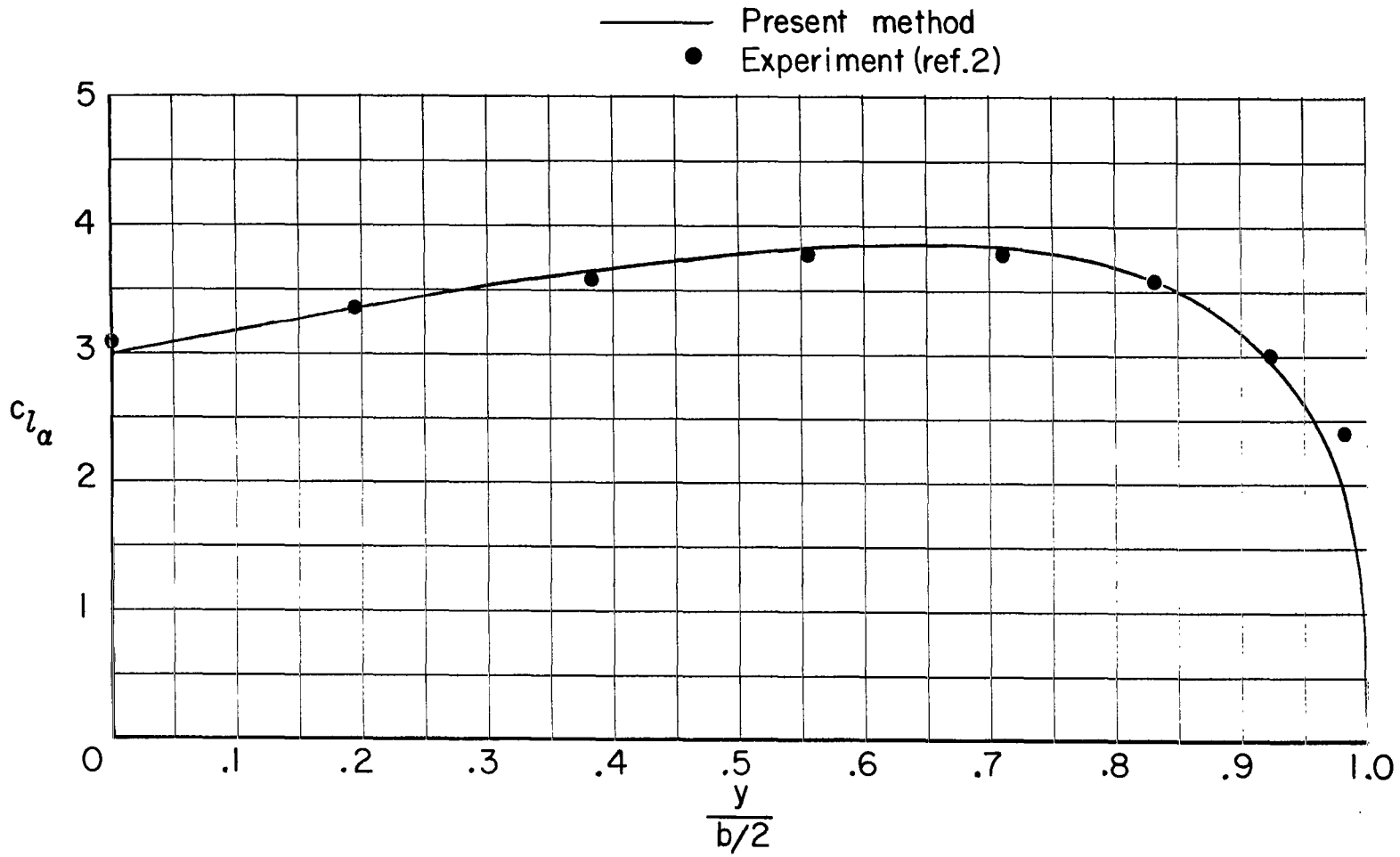

(b) Wing alone.

Figure 5.- Concluded.

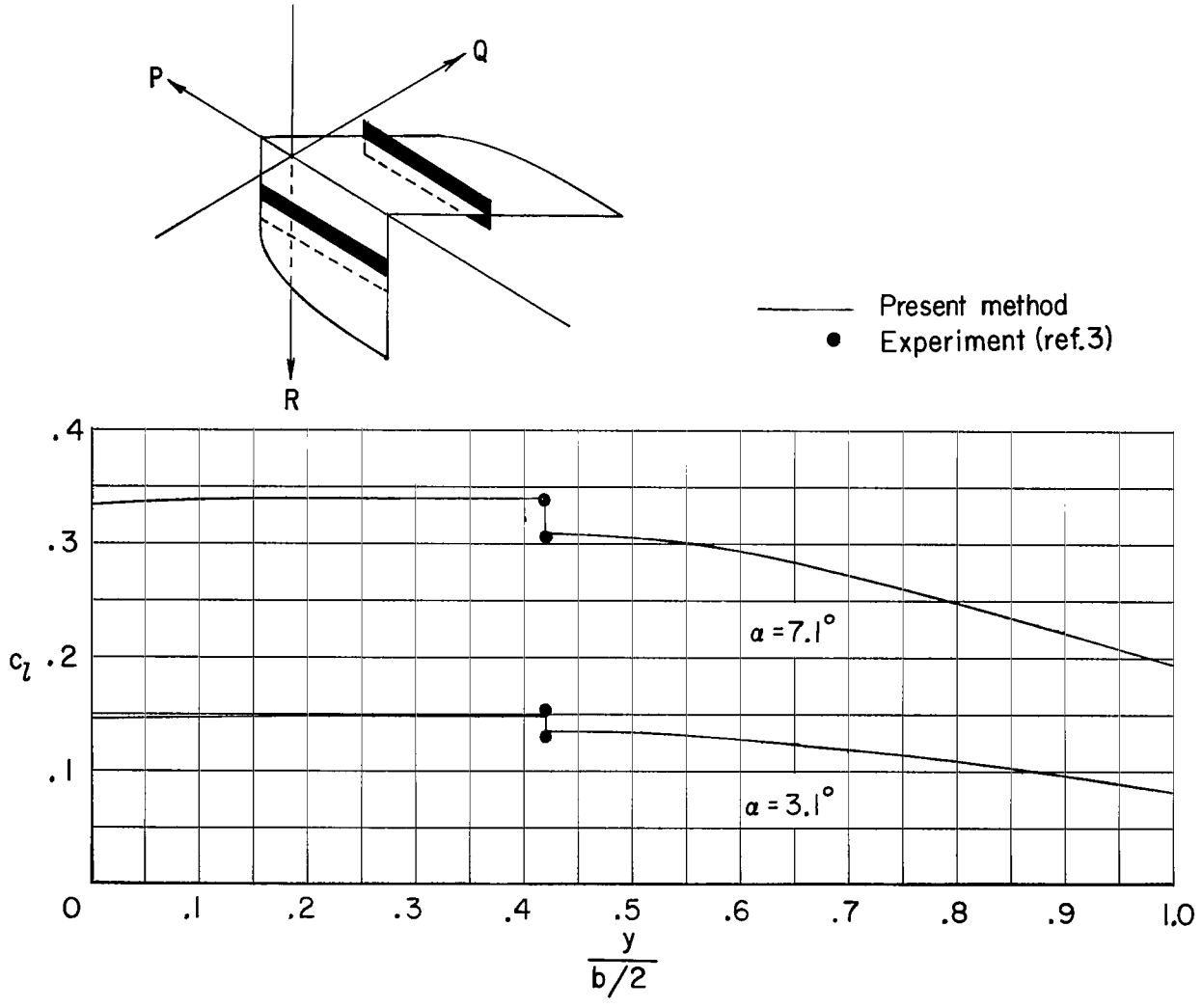

(a) Wing and fence.

Figure 6.- Effect of fence on section lift coefficient as calculated by present method and as indicated by experimental data of reference 3. $\Lambda_W = 45^0$; $A_W = 2.0$; $l = 0.12\frac{b}{2}$ (above and below the wing); $\eta = 0.42\frac{b}{2}$; $M_\infty \approx 0.1$; $s = 0.020\frac{b}{2}$.

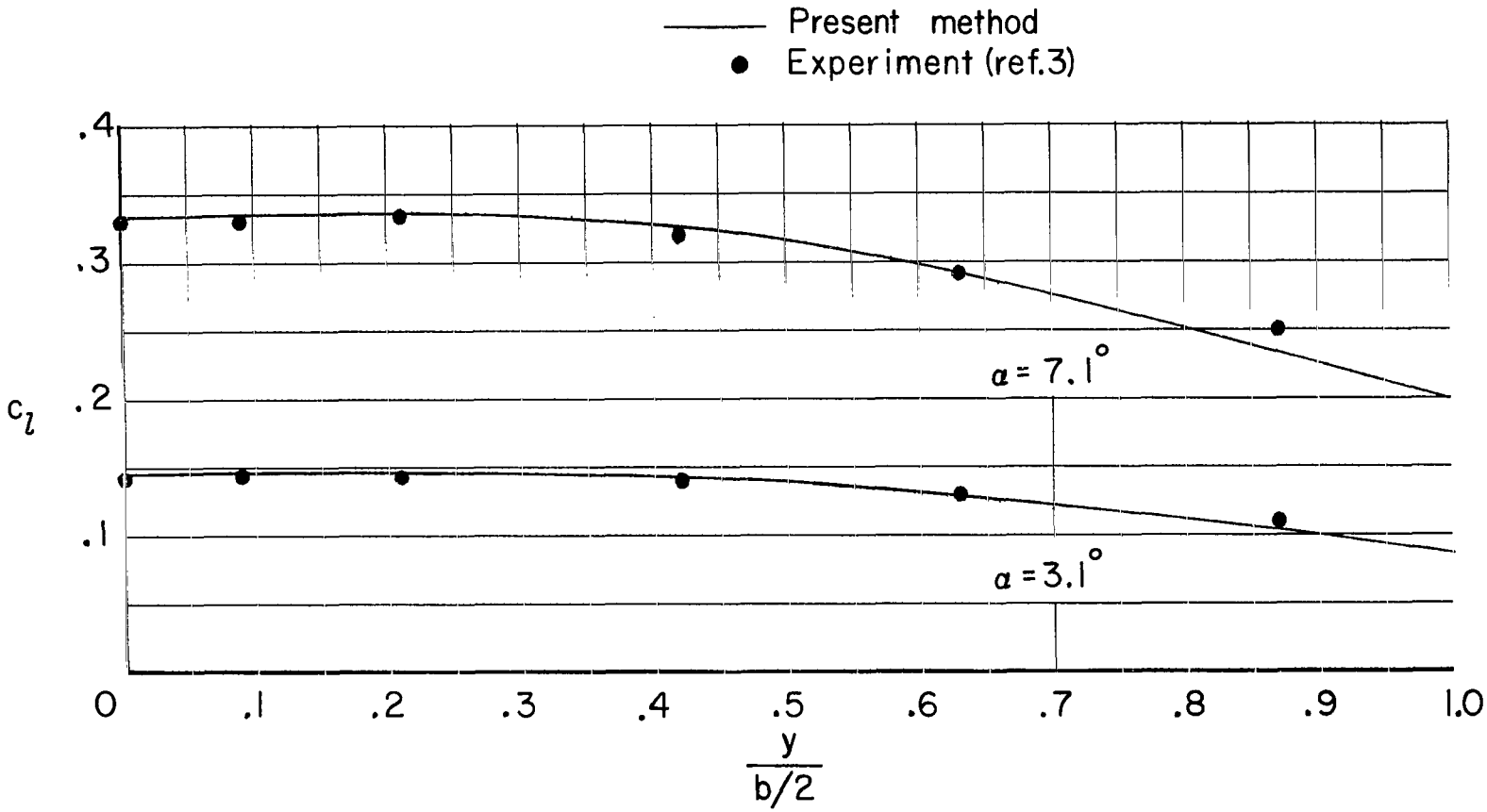

(b) Wing alone.

Figure 6.- Concluded.

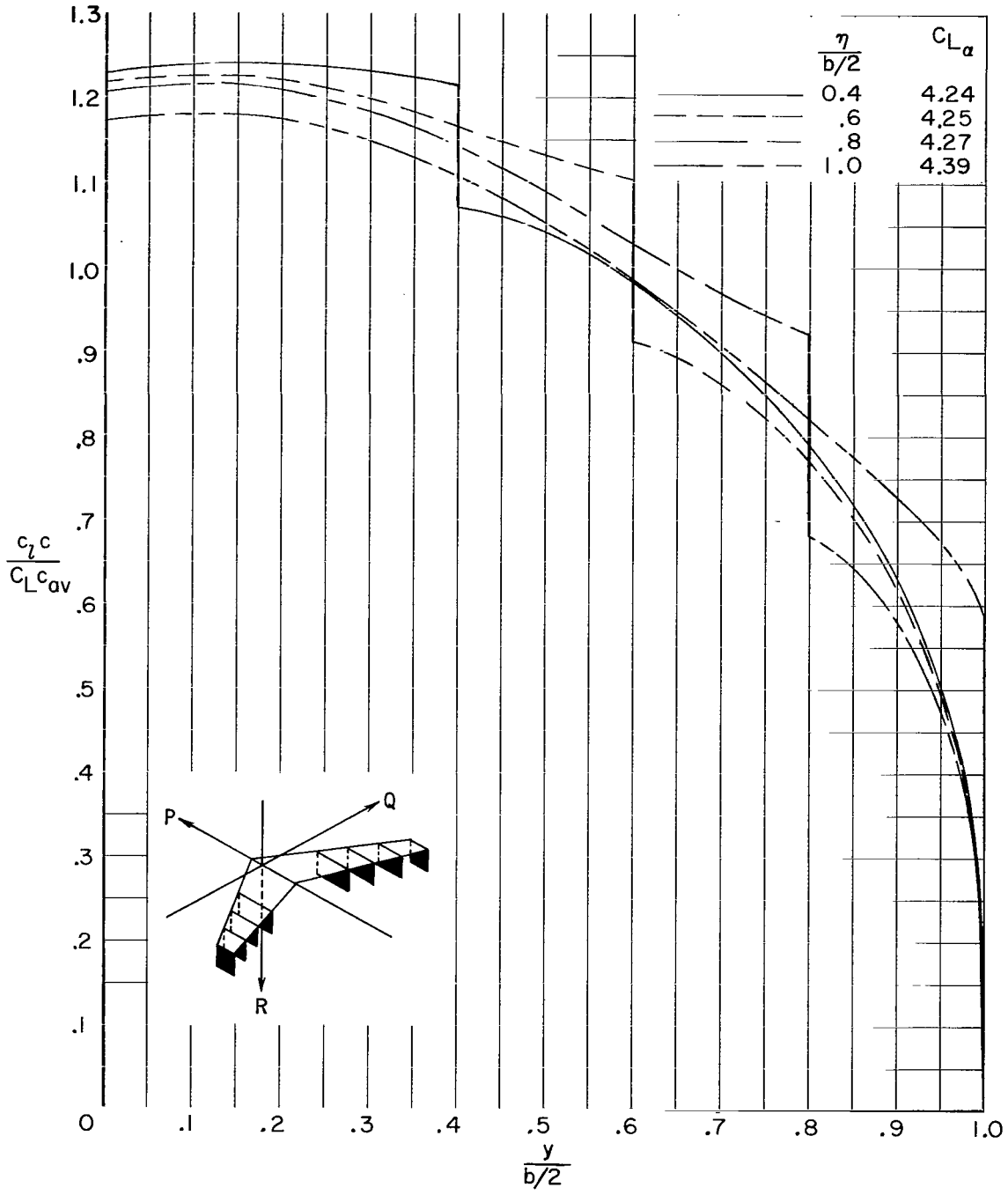

(a) Wing.

Figure 7.- Effect of vertical-surface location on wing and vertical-surface loading. $\Lambda_W = 30^0$; $A_W = 6.67$; $\lambda_W = 0.33$; $\Lambda_{VS} = 0^0$; $l = 0.2\frac{b}{2}$; $M_\infty = 0.0$; $s = 0.0250\frac{b}{2}$.

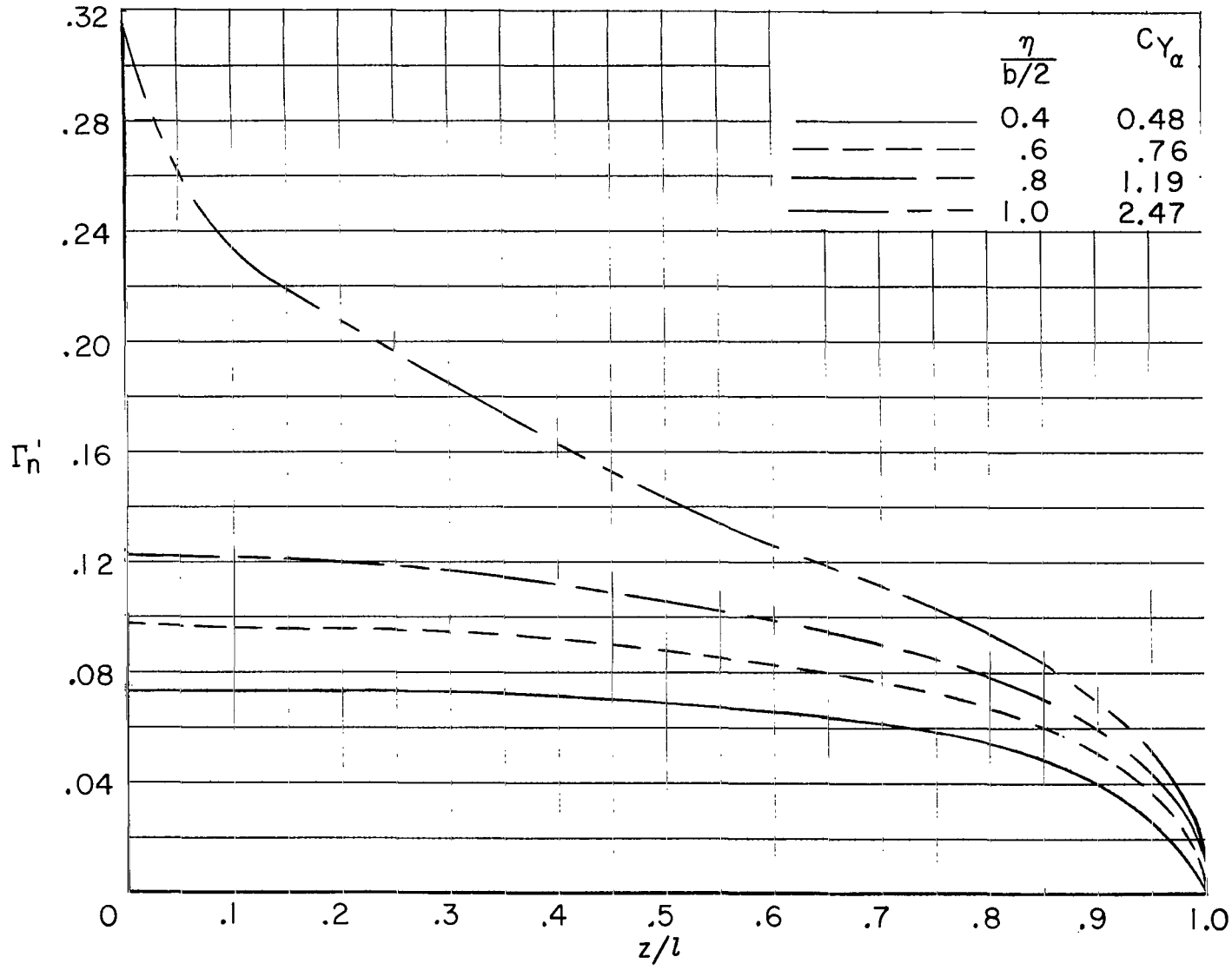

(b) Vertical surfaces; α = 1 radian.

Figure 7.- Concluded.

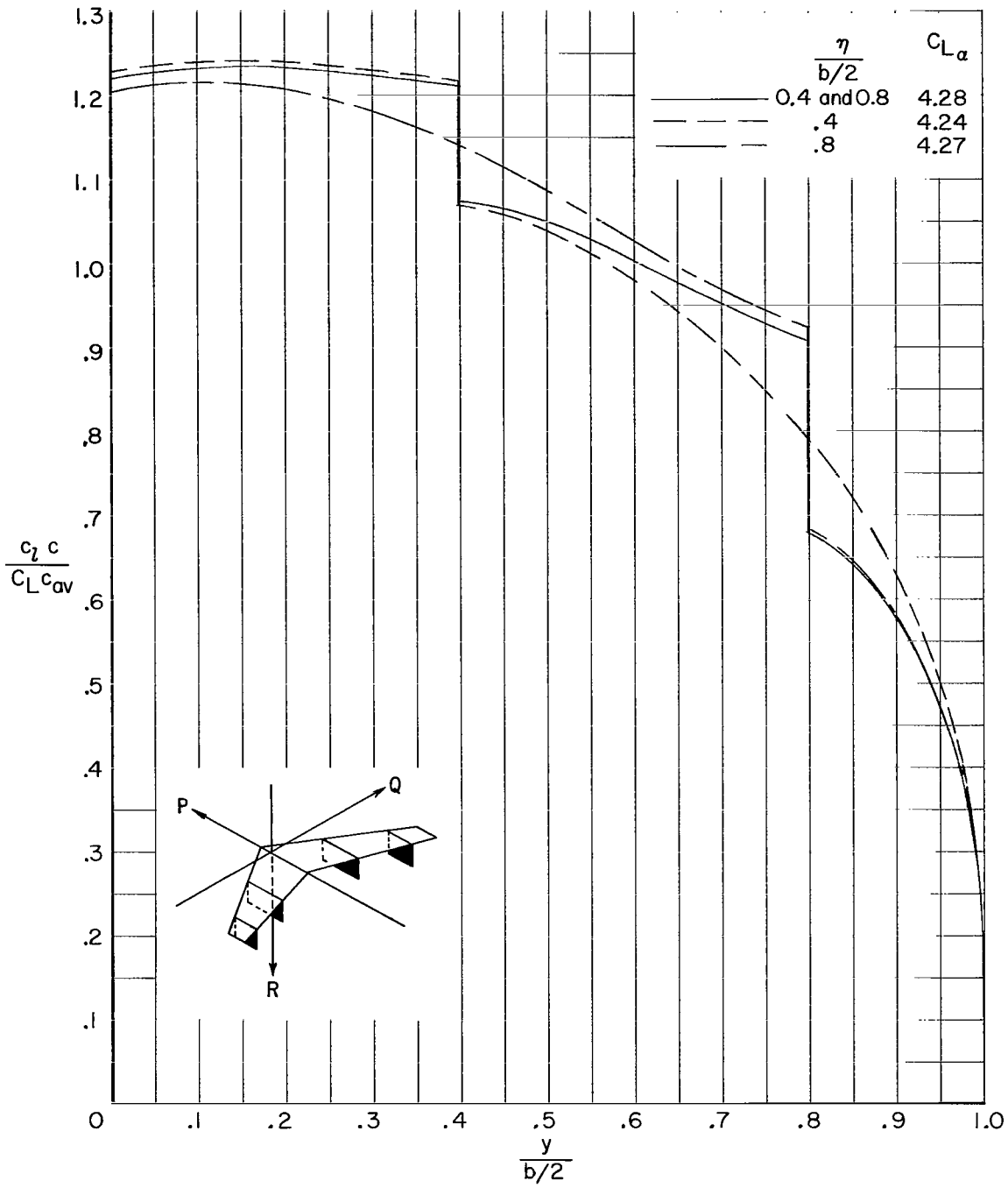

(a) Wing.

Figure 8.- Effect of number of vertical surfaces on wing and vertical-surface loading. $\Lambda_W = 30^0$; $A_W = 6.67$; $\lambda_W = 0.33$; $\Lambda_{VS} = 0^0$; $l = 0.2\frac{b}{2}$; $M_\infty = 0.0$; $s = 0.0250\frac{b}{2}$.

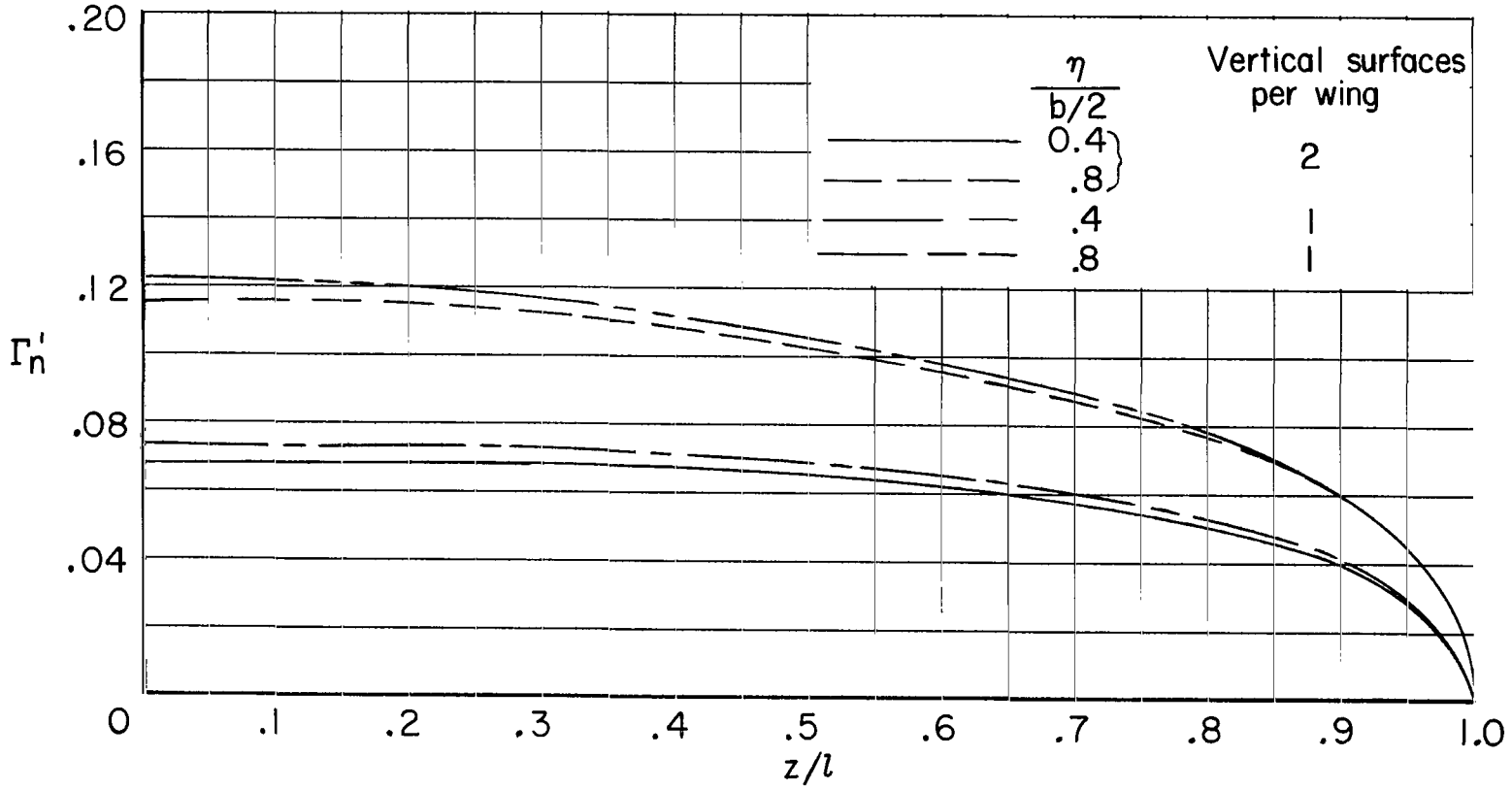

(b) Vertical surfaces; α = 1 radian.

Figure 8.- Concluded.

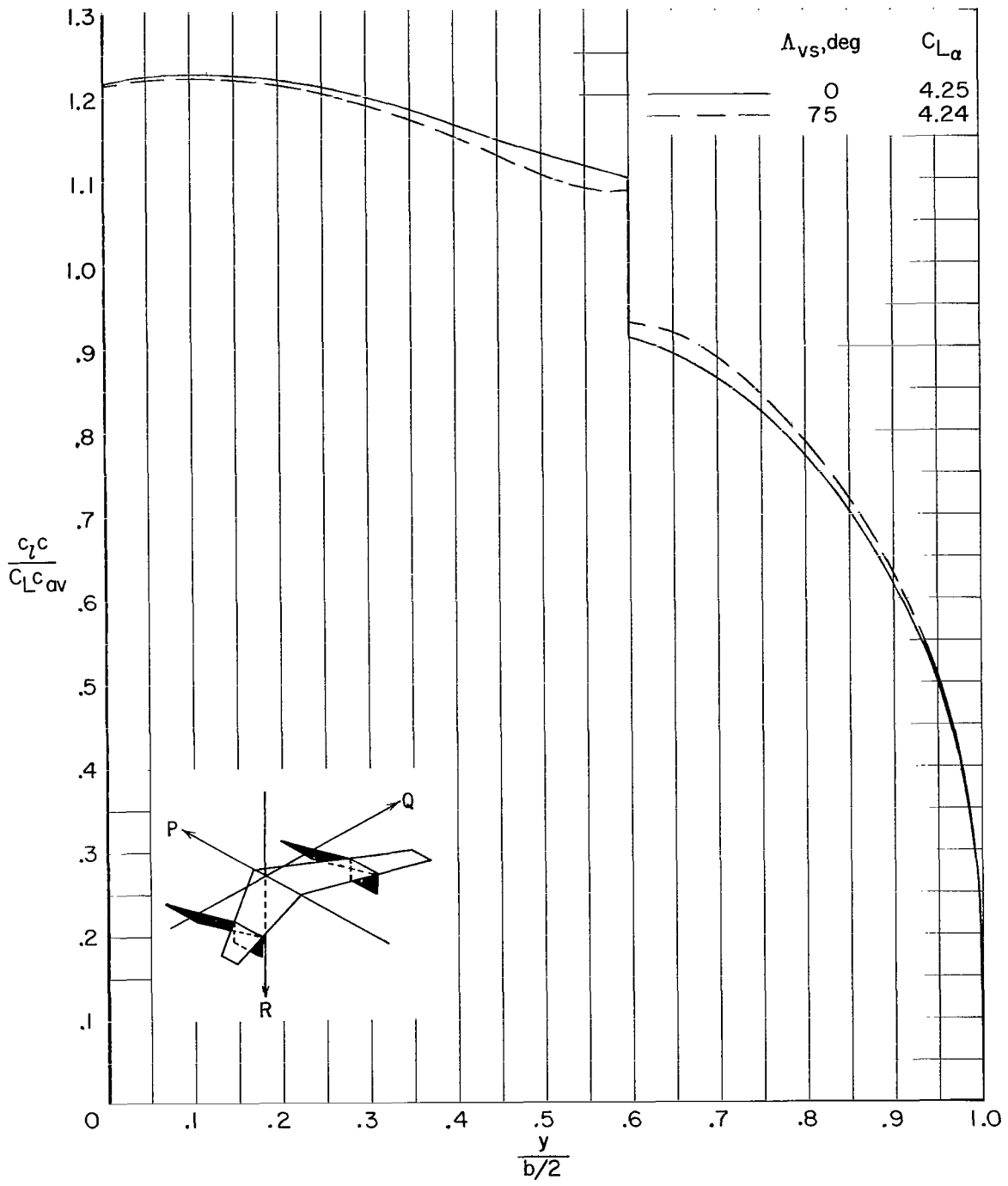

(a) Wing.

Figure 9.- Effect of vertical-surface sweep on wing and vertical-surface loading. $\Lambda_W = 30^o$; $A_W = 6.67$; $\lambda_W = 0.33$; $l = 0.2\frac{b}{2}$; $\eta = 0.6\frac{b}{2}$; $M_\infty = 0.0$; $s = 0.0250\frac{b}{2}$.

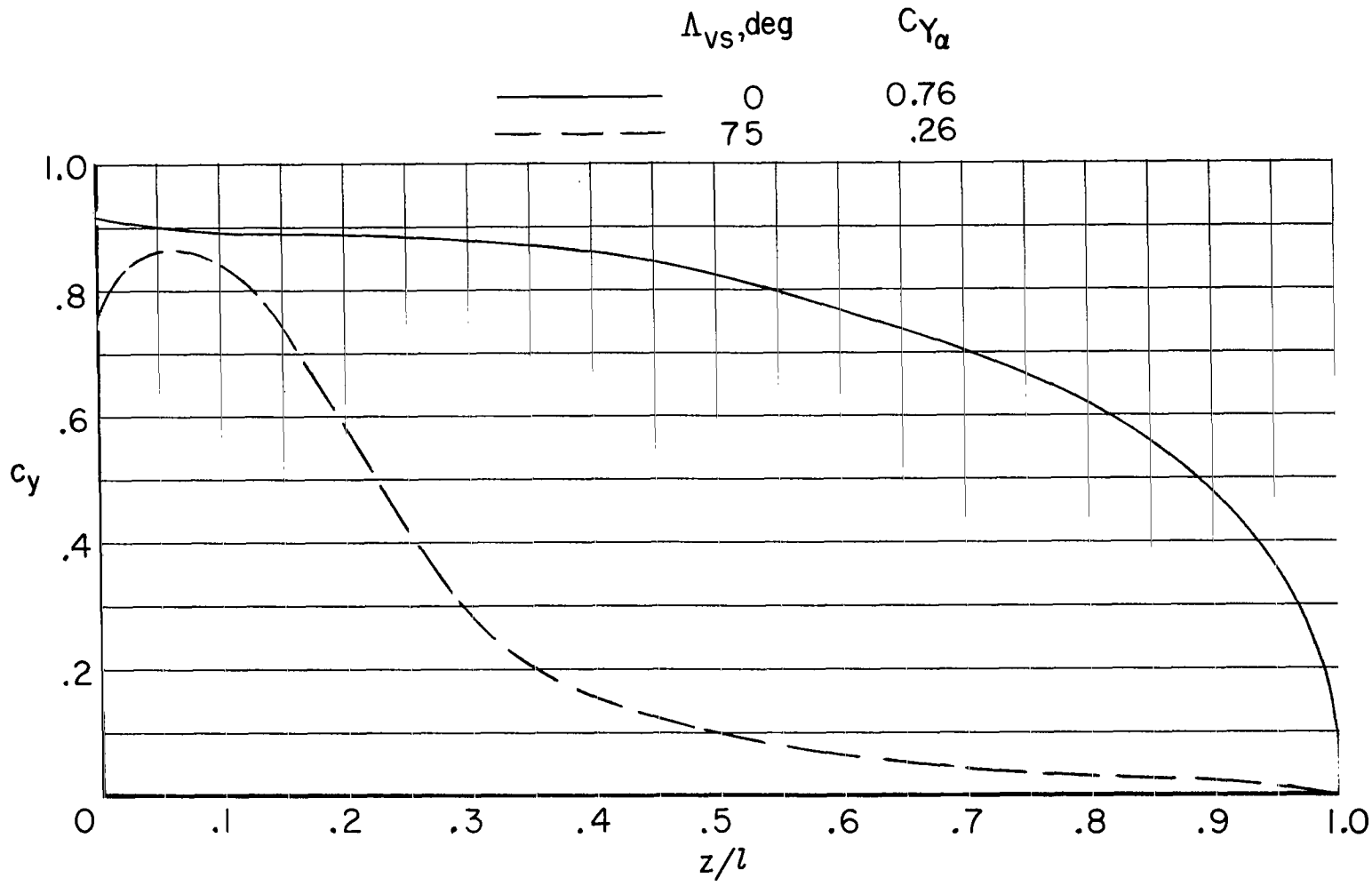

(b) Vertical surfaces; α = 1 radian.

Figure 9.- Concluded.

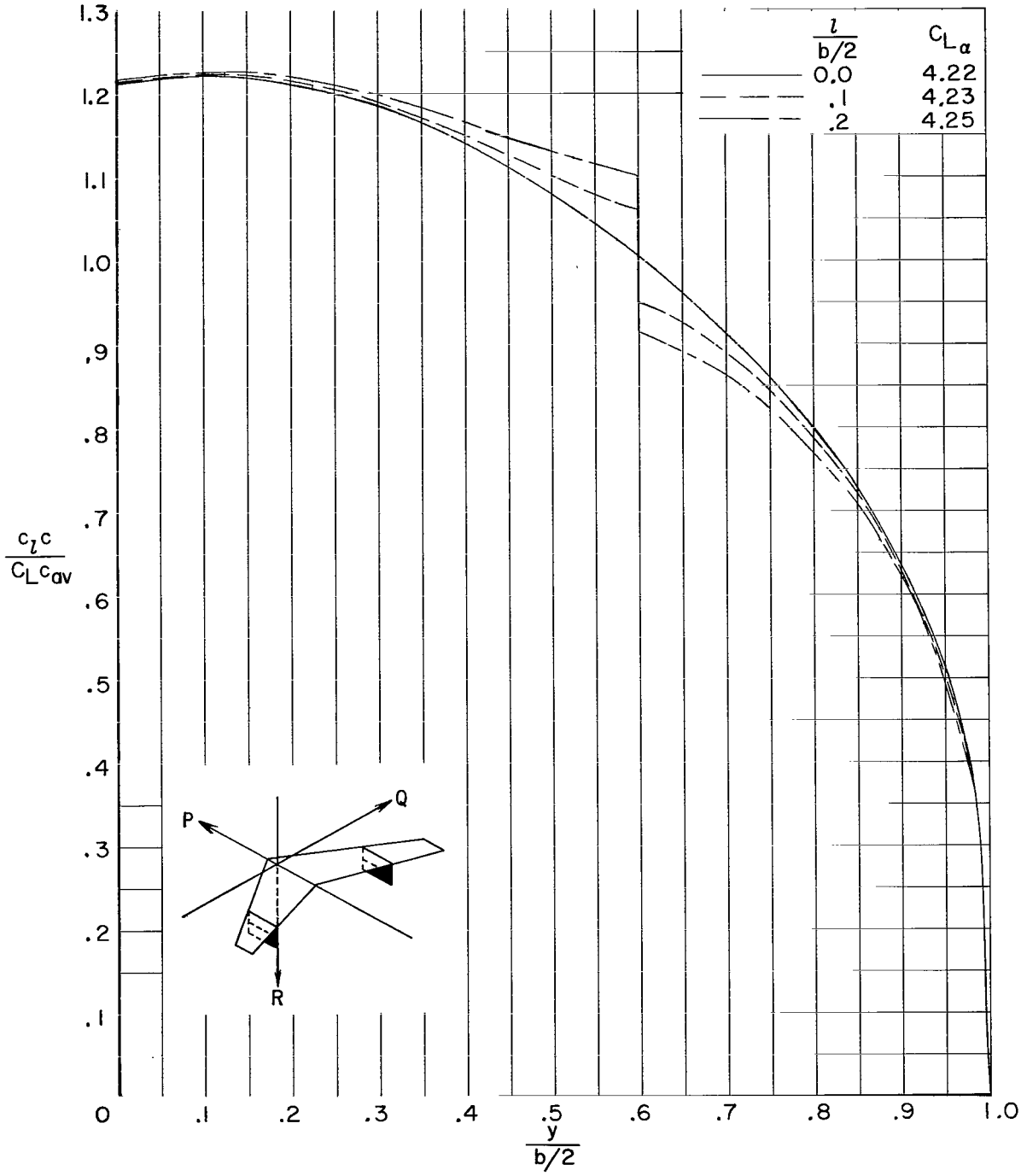

(a) Wing.

Figure 10.- Effect of vertical-surface height on wing and vertical-surface loading. $\Lambda_W = 30^0$; $A_W = 6.67$; $\lambda_W = 0.33$; $\Lambda_{VS} = 0^0$; $\eta = 0.6\frac{b}{2}$; $M_\infty = 0.0$; $s = 0.0250\frac{b}{2}$.

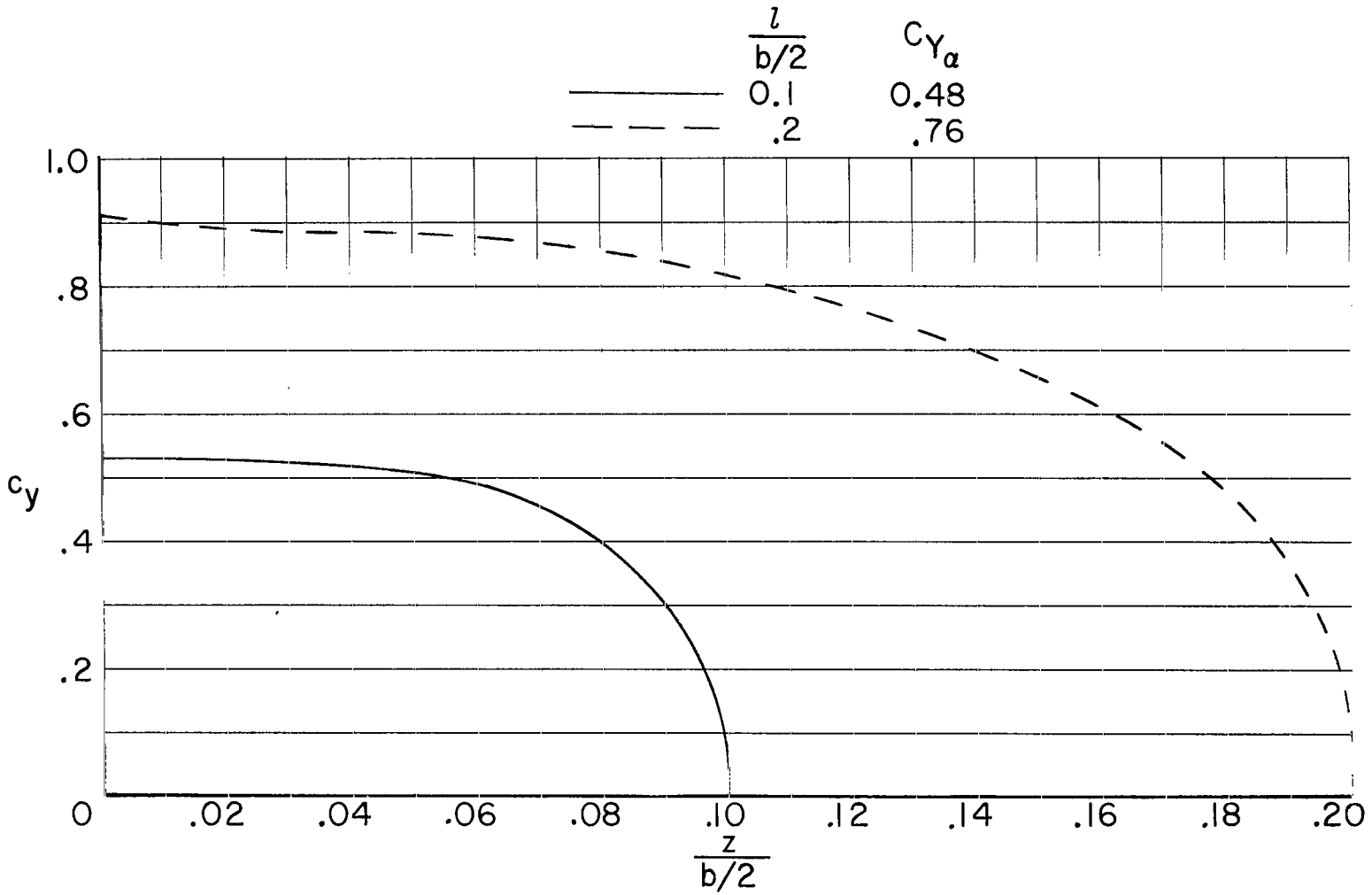

(b) Vertical surfaces; $\alpha = 1$ radian.

Figure 10.- Concluded.

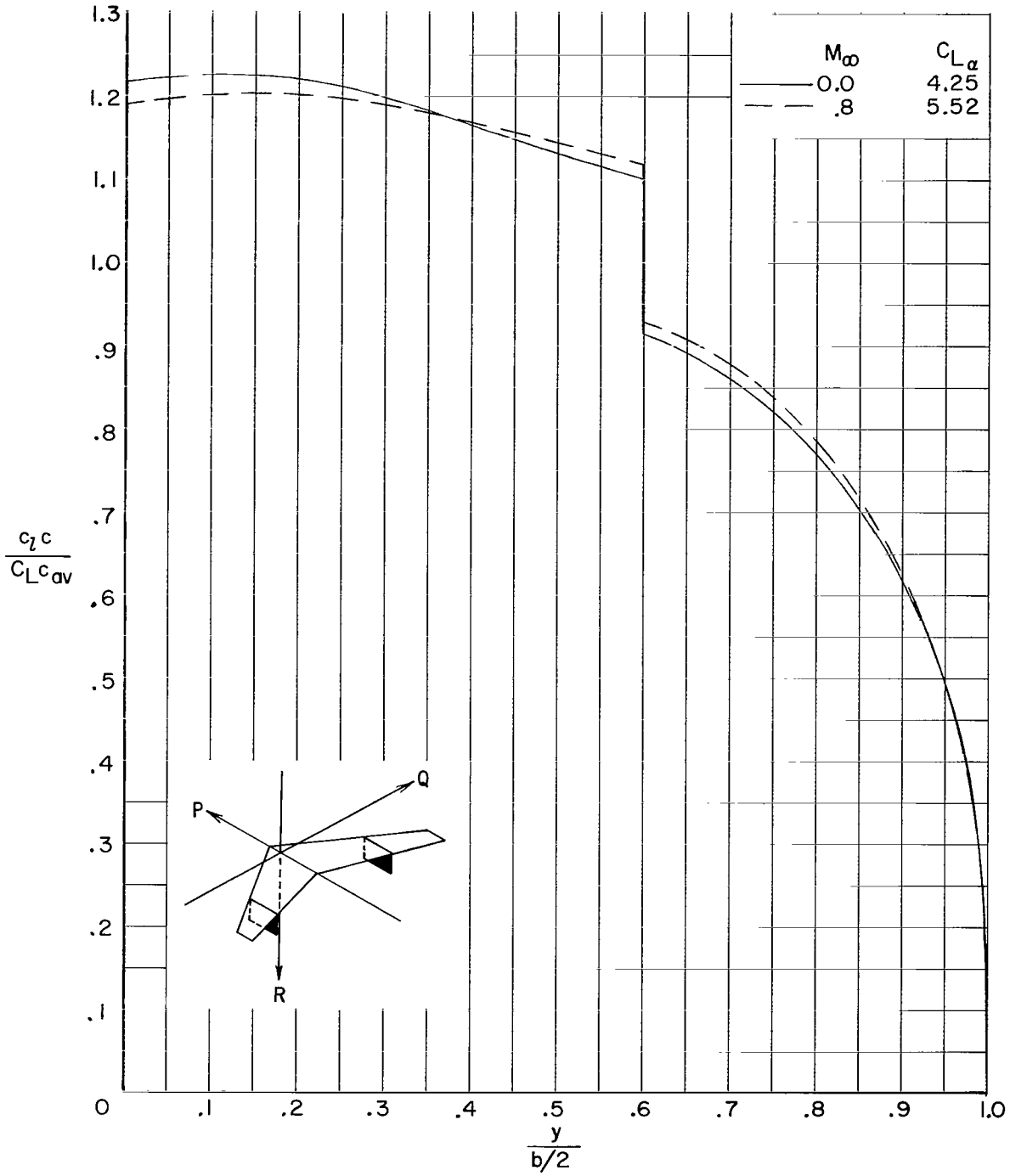

(a) Wing.

Figure 11.- Effect of Mach number on wing and vertical-surface loading. $\Lambda_W = 30^0$; $A_W = 6.67$; $\lambda_W = 0.33$; $\Lambda_{VS} = 0^0$; $l = 0.2\frac{b}{2}$; $\eta = 0.6\frac{b}{2}$; $s = 0.0250\frac{b}{2}$.

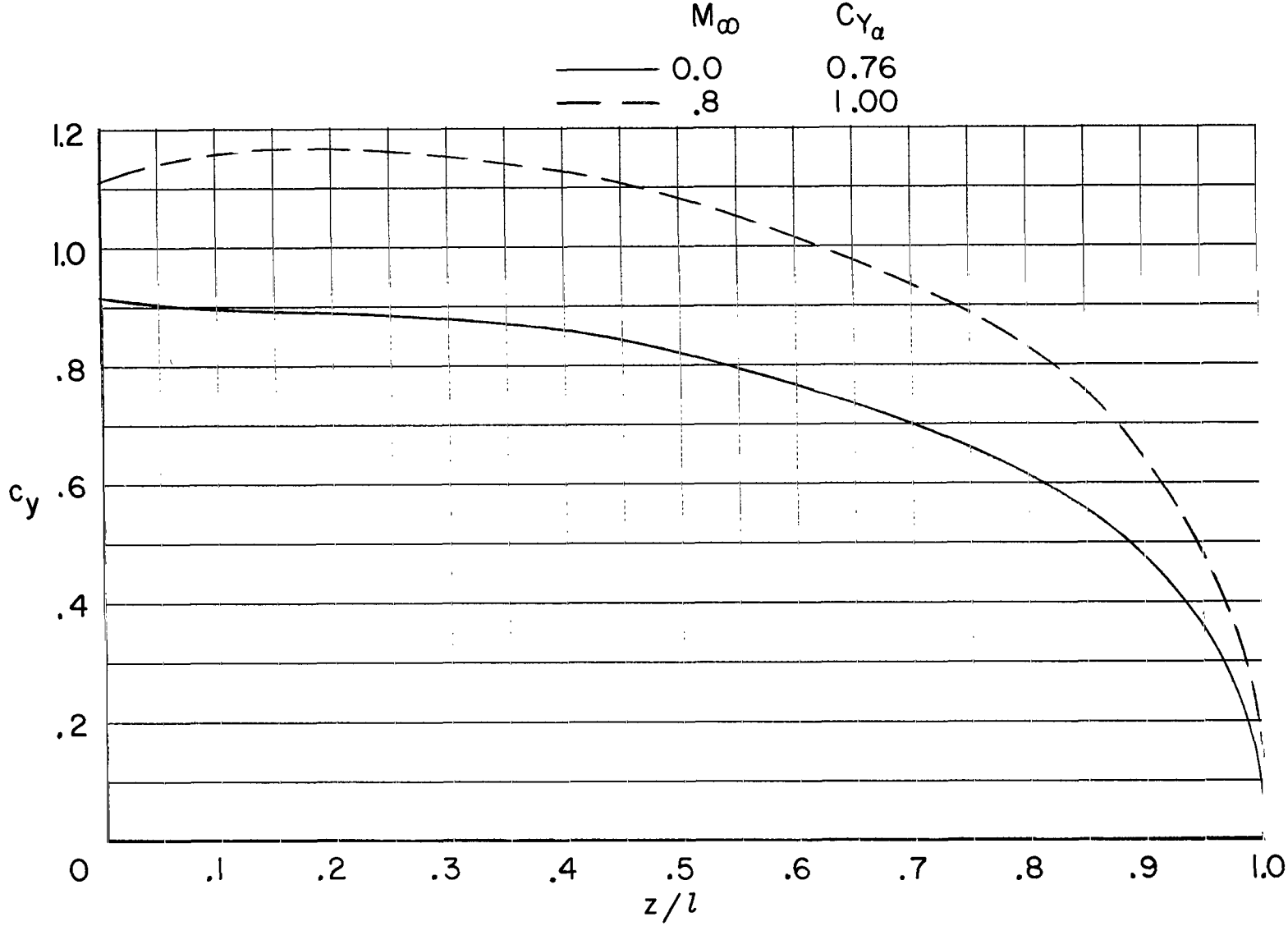

(b) Vertical surfaces; α = 1 radian.

Figure 11.- Concluded.

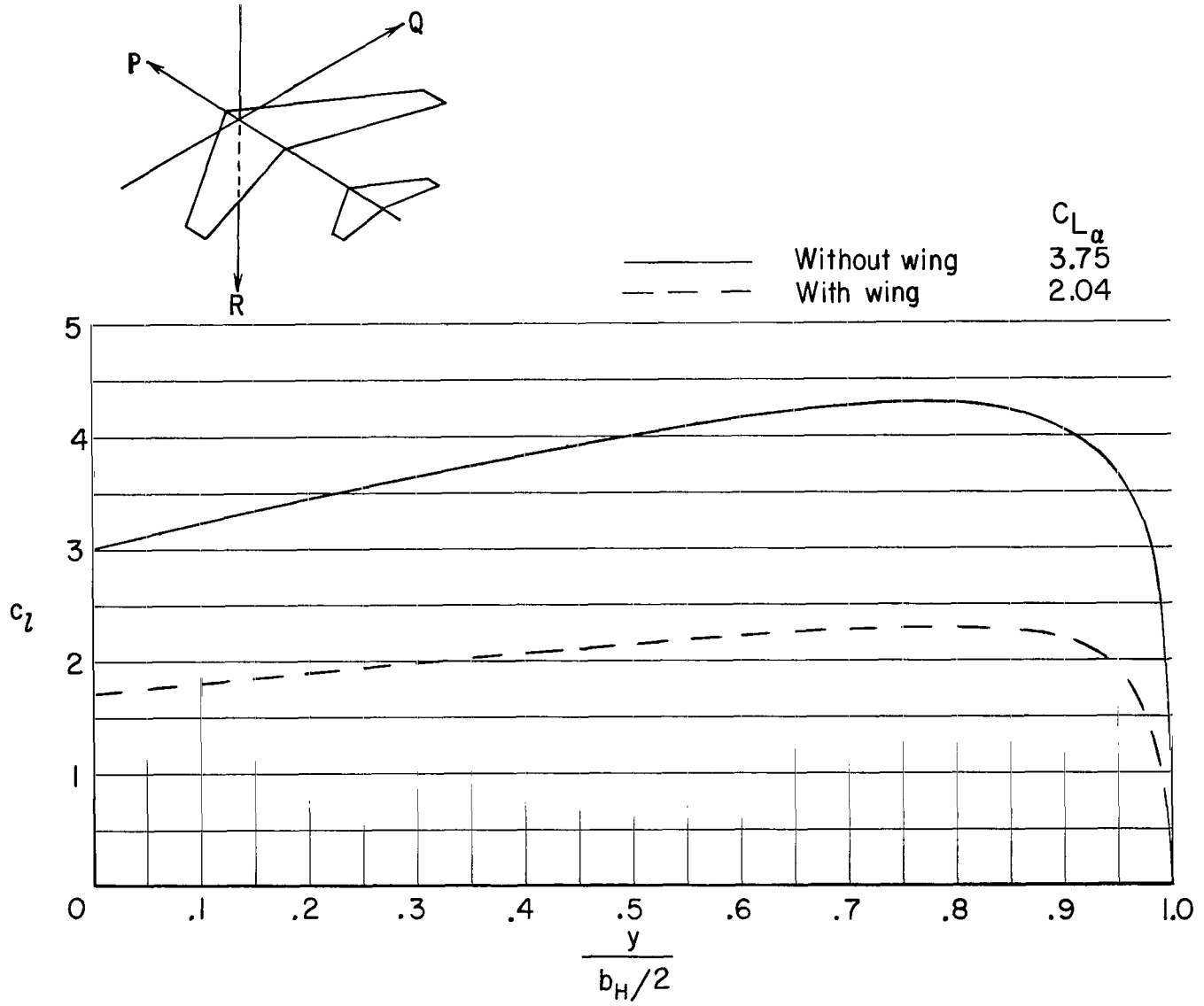

Figure 12.- Effect of wing wake on horizontal-tail lift distribution. $\Lambda_W = 30^0$; $A_W = 6.67$; $\lambda_W = 0.33$; $\Lambda_H = 30^0$; $A_H = 4.26$; $\lambda_H = 0.33$; $b_H/b = 0.4$; $\Delta\xi = -b/2$; $\Delta\zeta = 0.0$; $M_\infty = 0.0$; $\alpha = 1$ radian; $s = 0.0250\frac{b}{2}$.

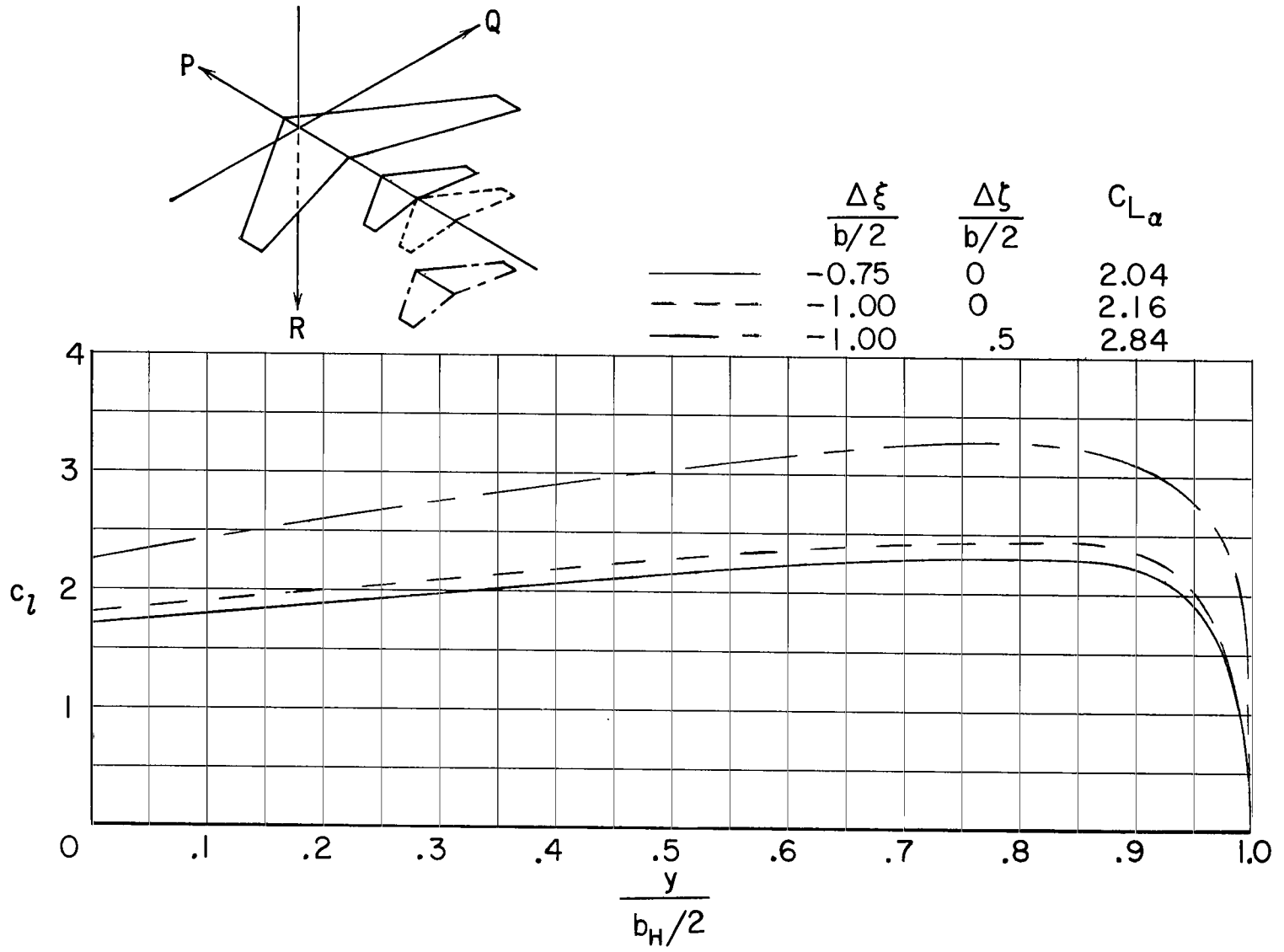

Figure 13.- Effect of horizontal-tail location behind wing on lift distribution of horizontal tail. $\Lambda_W = 30^0$; $A_W = 6.67$; $\lambda_W = 0.33$; $\Lambda_H = 30^0$; $A_H = 4.26$; $\lambda_H = 0.33$; $b_H/b = 0.4$; $M_\infty = 0.0$; $\alpha = 1$ radian; $s = 0.0250\frac{b}{2}$.

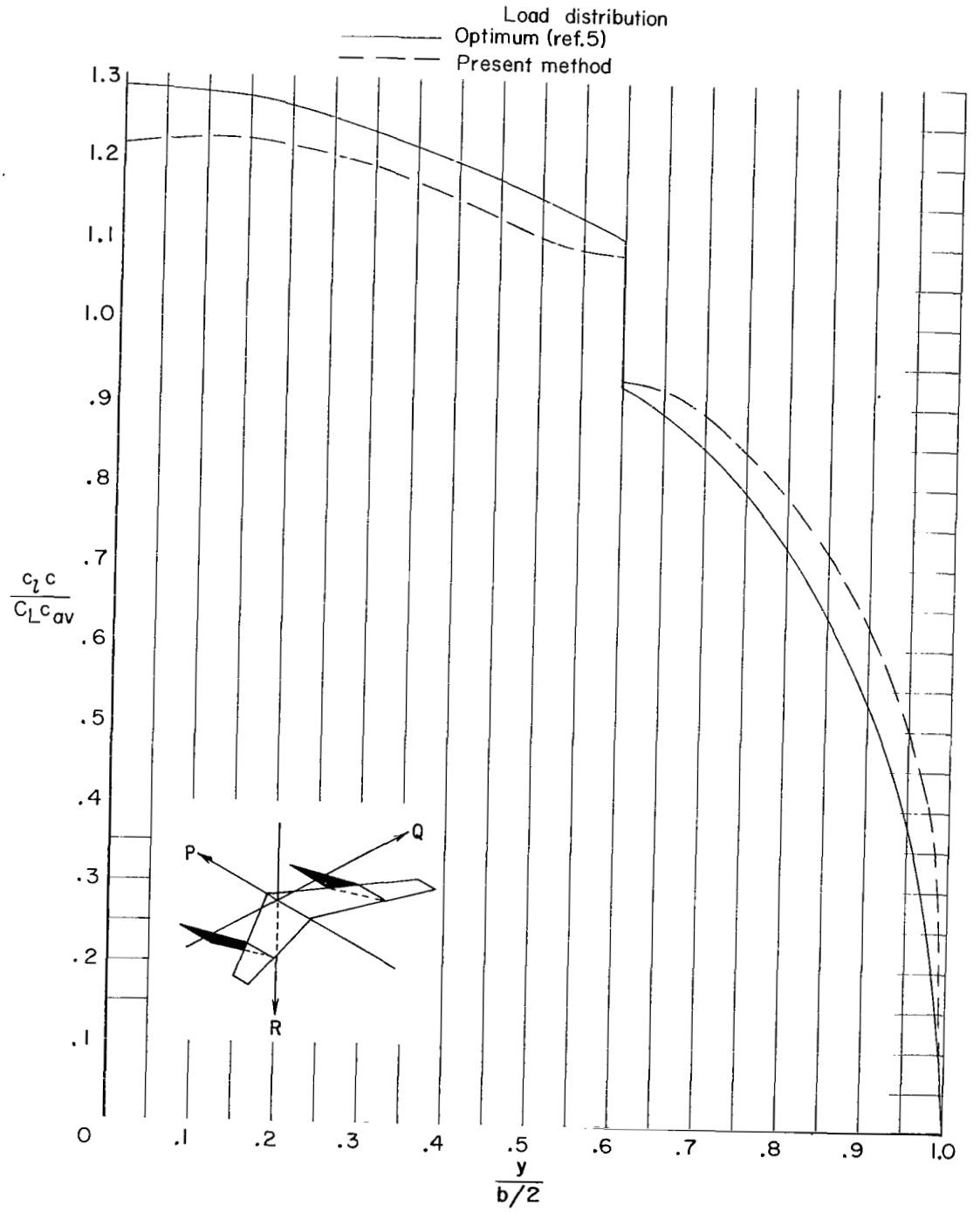

(a) Wing.

Figure 14.- Comparison of wing and vertical-surface loadings calculated by using present method with optimum loading of reference 5. $\Lambda_W = 30^0$; $A_W = 6.67$; $\lambda_W = 0.33$; $\Lambda_{VS} = 75^0$; $l = 0.2\frac{b}{2}$; $\eta = 0.6\frac{b}{2}$; $M_\infty = 0.0$; $s = 0.0250\frac{b}{2}$.

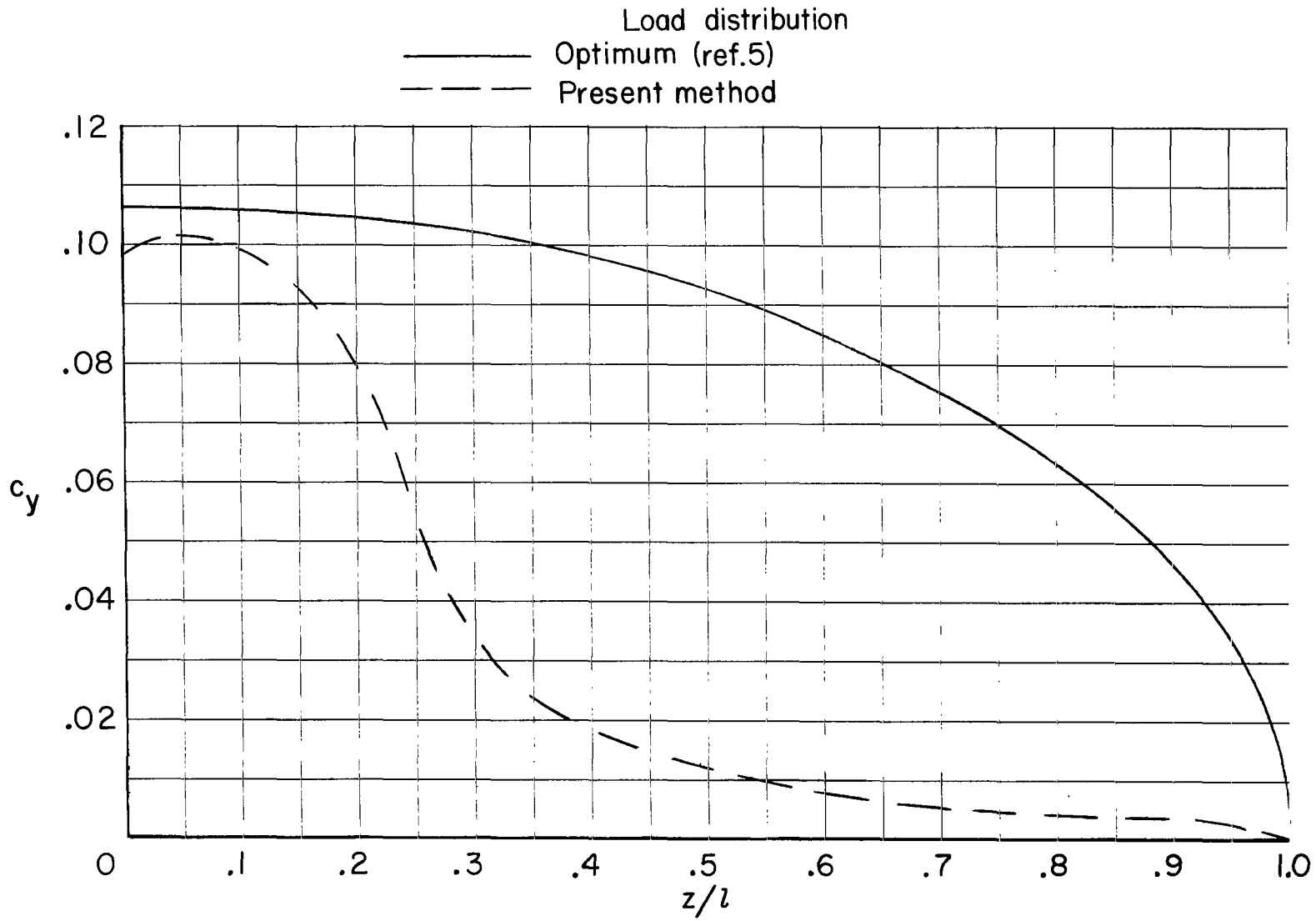

(b) Vertical surface; $C_L = 0.5$.

Figure 14.- Concluded.

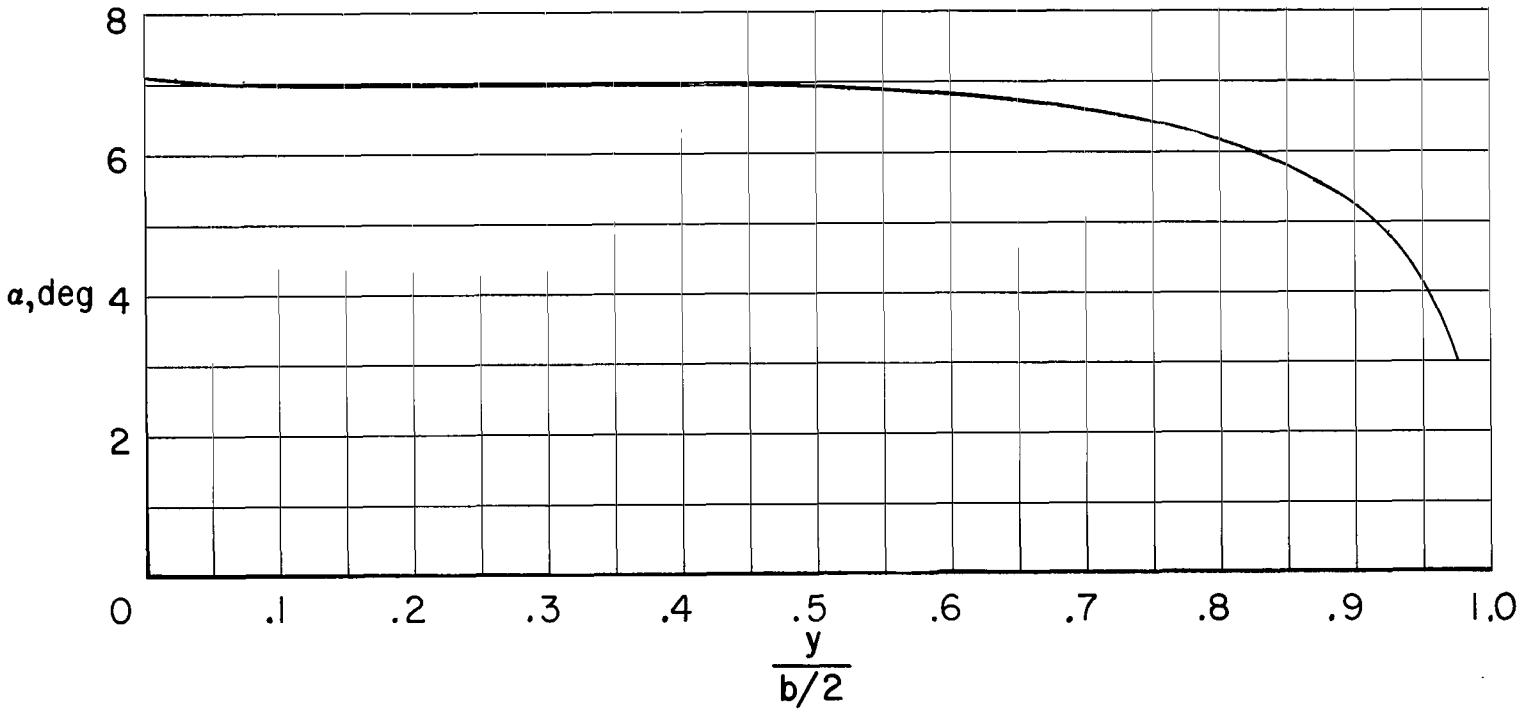

(a) Wing.

Figure 15.- Approximate wing incidence and vertical-surface deflection required to achieve optimum load distribution. $C_L = 0.5$; $\Lambda_W = 30^0$; $A_W = 6.67$; $\lambda_W = 0.33$; $\Lambda_{VS} = 75^0$; $l = 0.2\frac{b}{2}$; $\eta = 0.6\frac{b}{2}$; $M_\infty = 0.0$; $s = 0.0250\frac{b}{2}$.

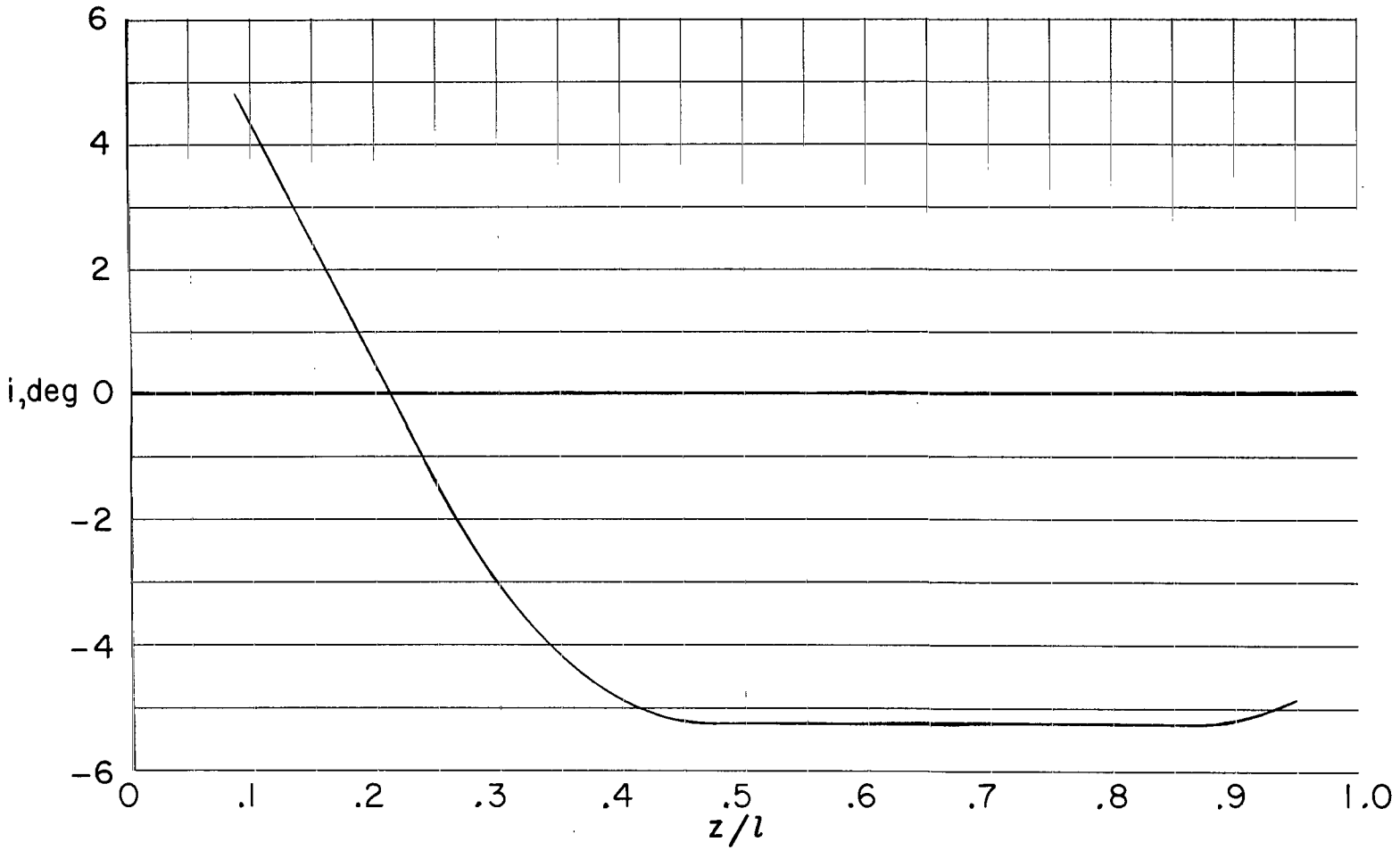

(b) Vertical surface. (+i indicates leading edge of vertical surface canted outboard.)

Figure 15.- Concluded.

NATIONAL AERONAUTICS AND SPACE ADMINISTRATION
WASHINGTON, D. C. 20546
OFFICIAL BUSINESS

FIRST CLASS MAIL

POSTAGE AND FEES PAID
NATIONAL AERONAUTICS AND
TION

"The aeronautical and space activities of the United States shall be conducted so as to contribute . . . to the expansion of human knowledge of phenomena in the atmosphere and space. The Administration shall provide for the widest practicable and appropriate dissemination of information concerning its activities and the results thereof."

—NATIONAL AERONAUTICS AND SPACE ACT OF 1958

NASA SCIENTIFIC AND TECHNICAL PUBLICATIONS

TECHNICAL REPORTS: Scientific and technical information considered important, complete, and a lasting contribution to existing knowledge.

TECHNICAL NOTES: Information less broad in scope but nevertheless of importance as a contribution to existing knowledge.

TECHNICAL MEMORANDUMS: Information receiving limited distribution because of preliminary data, security classification, or other reasons.

CONTRACTOR REPORTS: Scientific and technical information generated under a NASA contract or grant and considered an important contribution to existing knowledge.

TECHNICAL TRANSLATIONS: Information published in a foreign language considered to merit NASA distribution in English.

SPECIAL PUBLICATIONS: Information derived from or of value to NASA activities. Publications include conference proceedings, monographs, data compilations, handbooks, sourcebooks, and special bibliographies.

TECHNOLOGY UTILIZATION PUBLICATIONS: Information on technology used by NASA that may be of particular interest in commercial and other non-aerospace applications. Publications include Tech Briefs, Technology Utilization Reports and Notes, and Technology Surveys.

Details on the availability of these publications may be obtained from:

SCIENTIFIC AND TECHNICAL INFORMATION DIVISION

NATIONAL AERONAUTICS AND SPACE ADMINISTRATION

Washington, D.C. 20546